Upper Mantle Pollution during Afar Plume-Continental Rift Interaction

Tyrone O. Rooney, Barry Hanan, David W. Graham, Tanya Furman, Janne Blichert-Toft, Jean-Guy Schilling

HAL Id: insu-00673476

https://hal-insu.archives-ouvertes.fr/insu-00673476

Submitted on 20 Feb 2013

Upper Mantle Pollution during Afar Plume–Continental Rift Interaction

TYRONE O. ROONEY[1], BARRY B. HANAN[2]*, DAVID W. GRAHAM[3], TANYA FURMAN[4], JANNE BLICHERT-TOFT[5] AND JEAN-GUY SCHILLING[6]

[1]DEPARTMENT OF GEOLOGICAL SCIENCES, MICHIGAN STATE UNIVERSITY, EAST LANSING, MI 48824, USA

[2]DEPARTMENT OF GEOLOGICAL SCIENCES, SAN DIEGO STATE UNIVERSITY, SAN DIEGO, CA 92182-1020, USA

[3]COLLEGE OF OCEANIC AND ATMOSPHERIC SCIENCES, OREGON STATE UNIVERSITY, CORVALLIS, OR 97331, USA

[4]DEPARTMENT OF GEOSCIENCES, PENNSYLVANIA STATE UNIVERSITY, UNIVERSITY PARK, PA 16802, USA

[5]LABORATOIRE DE GÉOLOGIE DE LYON, ECOLE NORMALE SUPÉRIEURE DE LYON AND UNIVERSITÉ CLAUDE BERNARD LYON 1, CNRS UMR 5276, 46 ALLÉE D'ITALIE, 69007 LYON, FRANCE

[6]GRADUATE SCHOOL OF OCEANOGRAPHY, UNIVERSITY OF RHODE ISLAND, KINGSTON, RI 02881, USA

New Pb, Sr, Nd, Hf, and He isotope data for Quaternary basalts, erupted from Debre Zeyit, Butajira, and the Wonji Fault Belt of the Main Ethiopian Rift, show systematic mixing relationships involving three distinct mantle sources. The Pb, Sr, Nd, and Hf isotopic arrays converge in a specific region of isotopic multi-space where they define the composition of the Afar mantle plume (centered about $^{206}Pb/^{204}Pb = 19\cdot5$, $^{87}Sr/^{86}Sr = 0\cdot7035$, $\varepsilon_{Nd} = +4\cdot6$, $\varepsilon_{Hf} = +9\cdot3$, $^{3}He/^{4}He > 15\ R_A$). This plume end-member has an identical composition to that observed previously in oceanic basalts. The distinct isotopic arrays for the various volcanic areas in the Main Ethiopian Rift vary spatially in a systematic manner, and may be viewed as pseudo-binary mixing arrays. This further suggests that the Afar mantle plume interacts with the local continental lithosphere and upper mantle asthenosphere (mid-ocean ridge basalt-like source) through an ordered sequence of mixing events. Simple mixing models require that the mass proportions of continental lithosphere and upper mantle involved in magma generation must be nearly constant within each volcanic area, but that the proportion of plume material decreases regularly with distance southwestward along the Main Ethiopian Rift, away from the central axis of the plume. This systematic behavior means that continental lithosphere can become detached and mixed into the shallow mantle prior to the flow of upwelling plume material beneath the developing rift system. Detachment and mixing into the asthenosphere during continental rift evolution is an important process for producing the range of ambient upper mantle compositions sampled by mid-ocean ridge volcanism away from island hotspots.

INTRODUCTION

Mantle plumes, anomalously hot and buoyant upwellings from the deep mantle, can strongly influence the chemical composition of basalts erupted at spreading ocean ridges (Morgan, 1972; Schilling, 1973a, 1985; Hanan et al., 1986; Detrick et al., 2002) as well as those in continental settings (Morgan, 1971; Burke & Wilson, 1972; Watts, 1976; Crough, 1978; Courtney & White, 1986; Campbell & Griffiths, 1990; McNutt & Judge, 1990; Griffiths & Campbell, 1991; Farnetani & Richards, 1994; Ingle et al., 2002; Ernst & Buchan, 2003; Jones & White, 2003; Camp & Ross, 2004; Pik et al., 2006; Saunders et al., 2007; Hanan et al., 2008; Camp & Hanan, 2008; Shervais & Hanan, 2008; Graham et al., 2009). Much of the spatial variation of Pb, Nd, Sr, and He isotopes in mid-ocean ridge basalts (MORB) from the South Atlantic appears to have been produced during broad radial dispersion of isotopically distinct

*Corresponding author. Telephone: 1 619 594-6710. Fax: 1 619 594-7161. E-mail: bhanan@mail.sdsu.edu

plume material into the asthenosphere during rifting and formation of the ocean basin, prior to when the plumes were over-ridden (in the fixed hotspot reference frame; Duncan, 1981) by the migrating Mid-Atlantic Ridge (Hanan *et al.*, 1986; Graham *et al.*, 1992). Thus, one explanation for the observed range of upper mantle compositions is that it reflects isotopic heterogeneity introduced by hotspots derived from distinct source reservoirs in the deep mantle (e.g. Storey *et al.*, 1989). However, geochemical studies of MORB and continental basalts also indicate that the upper mantle has been polluted by continental lithosphere and/or lower crust (Arndt & Goldstein, 1989; Kamenetsky *et al.*, 2001; Hanan *et al.*, 2004; Carlson *et al.*, 2005; Escrig *et al.*, 2005; Class & le Roex, 2006; Goldstein *et al.*, 2008). The spectrum of isotopic signatures observed in ocean island (hotspot) basalts, ranging between EM I, EM II and HIMU (Zindler & Hart, 1986), is also observed in basalts and xenoliths that sample the continental lithosphere and lower continental crust (e.g. McKenzie & O'Nions, 1995). Therefore, a second explanation for the origin of isotopic heterogeneity in the upper mantle is that it reflects direct pollution and mixing with detached continental lithosphere. Here we address these two different possibilities (deep vs shallow sources of mantle isotopic heterogeneity) through isotopic characterization and modelling of the sources involved in plume–lithosphere interaction along the Main Ethiopian Rift. The Main Ethiopian Rift is the type example of a modern continental rift in a plume-influenced environment (Falcon *et al.*, 1970; Girdler, 1970; Schilling, 1973*b*), and provides a natural laboratory for studying the interaction of a mantle plume with the continental lithosphere.

The Red Sea, Gulf of Aden, and Main Ethiopian Rift meet in the Afar triangle, where they delineate three arms of a rift system that began at ∼30 Ma over the upwelling Afar mantle plume (Fig. 1; Hofmann *et al.*, 1997). The Main Ethiopian Rift is the least evolved of the three triple junction arms, is about 18 Myr younger than the Red Sea and Gulf of Aden rifts, and is thus not a primary feature of the Afar plume, but is instead related to plate kinematics (Wolfenden *et al.*, 2004). The Main Ethiopian Rift began to propagate north from the Turkana region, a zone previously rifted in the Mesozoic and again in the Cenozoic, at ∼11 Ma, coincident in time with the propagation of the Kenya Rift (Ebinger *et al.*, 2000).

Previous studies have described the isotopic diversity of the Main Ethiopian Rift magmas in terms of mixing between plume, depleted upper mantle, and continental lithosphere (Deniel *et al.*, 1994; Barrat *et al.*, 1998; Trua *et al.*, 1999; Rogers *et al.*, 2000; Furman, 2007), but only in very broad terms. Although the timing, extent and mechanisms of mixing between these mantle reservoirs are central to the development of an integrated geodynamic model of the rifting process, they have remained poorly understood. Schilling (1973*b*) and Schilling *et al.* (1992) reported rare earth element and Nd–Sr–Pb isotopic compositions of basalts dredged from along the Sheba Ridge in the Gulf of Aden and its extension into the Gulf of Tadjoura, and of subaerial basalts from the Asal Rift in eastern Afar (Fig. 1). This dataset provided an initial framework for interpreting melting processes associated with interaction of the Afar plume with the continental lithosphere and an emerging ocean basin. The mixing relationships (Schilling *et al.*, 1992) define three mantle source end-members interpreted as Pan-African continental lithosphere, the Afar mantle plume, and the depleted upper mantle (MORB asthenosphere source).

In this study we refine and extend the original three-component mixing model of Schilling *et al.* (1992) to the Butajira, Debre Zeyit, and Wonji Fault Belt regions of the Main Ethiopian Rift, three extensional zones that together form a 250 km transect along the Main Ethiopian Rift (Fig. 1, Table 1). We focus on Quaternary basalts having ages <1 Ma, and present new Pb, Nd, Sr, Hf, and He isotope results, as well as new Hf isotope data for the same Gulf of Aden sample suite previously analyzed for Pb, Nd, and Sr isotopes by Schilling *et al.* (1992; Table 2). Collectively, we use these new data to quantitatively characterize the distribution of mantle source reservoirs along the Main Ethiopian Rift portion of the East African Rift, their relative contribution to volcanism, and their sequence of mixing.

BACKGROUND
Sample selection

A subset of the most primitive Main Ethiopian Rift samples (6–10 wt % MgO) previously analyzed for major and trace elements (Rooney *et al.*, 2005, 2007, 2011; Furman *et al.*, 2006; Rooney, 2010) were selected for Hf, Sr, Nd, Pb ($n = 15$), and He ($n = 12$) isotopic analysis. The major element and trace element data for two samples, WFB-1026 and WFB-N-14, that were analyzed but not reported by Furman *et al.* (2006), are reported in Appendix Table A1. Hf isotope data are also reported for a suite of basalts dredged from the Sheba Ridge axis in the Gulf of Aden and its extension into the Gulf of Tadjoura, and for subaerial basalts from the Asal Rift of eastern Afar. The Pb, Sr, and Nd isotope data for these samples were reported by Schilling *et al.* (1992), and are the basis for the three-component mixing model proposed therein. The analytical details for the Main Ethiopian Rift and Gulf of Aden isotope data are given in the legends of Tables 1–3. The complete dataset is provided as Supplementary Data (available for downloading at http://www.petrology. oxfordjournals.org/).

Crustal contamination indicators (e.g. La/Nb and Ce/Pb) for the samples selected for isotopic analysis and modeling show no evidence for significant crustal assimilation
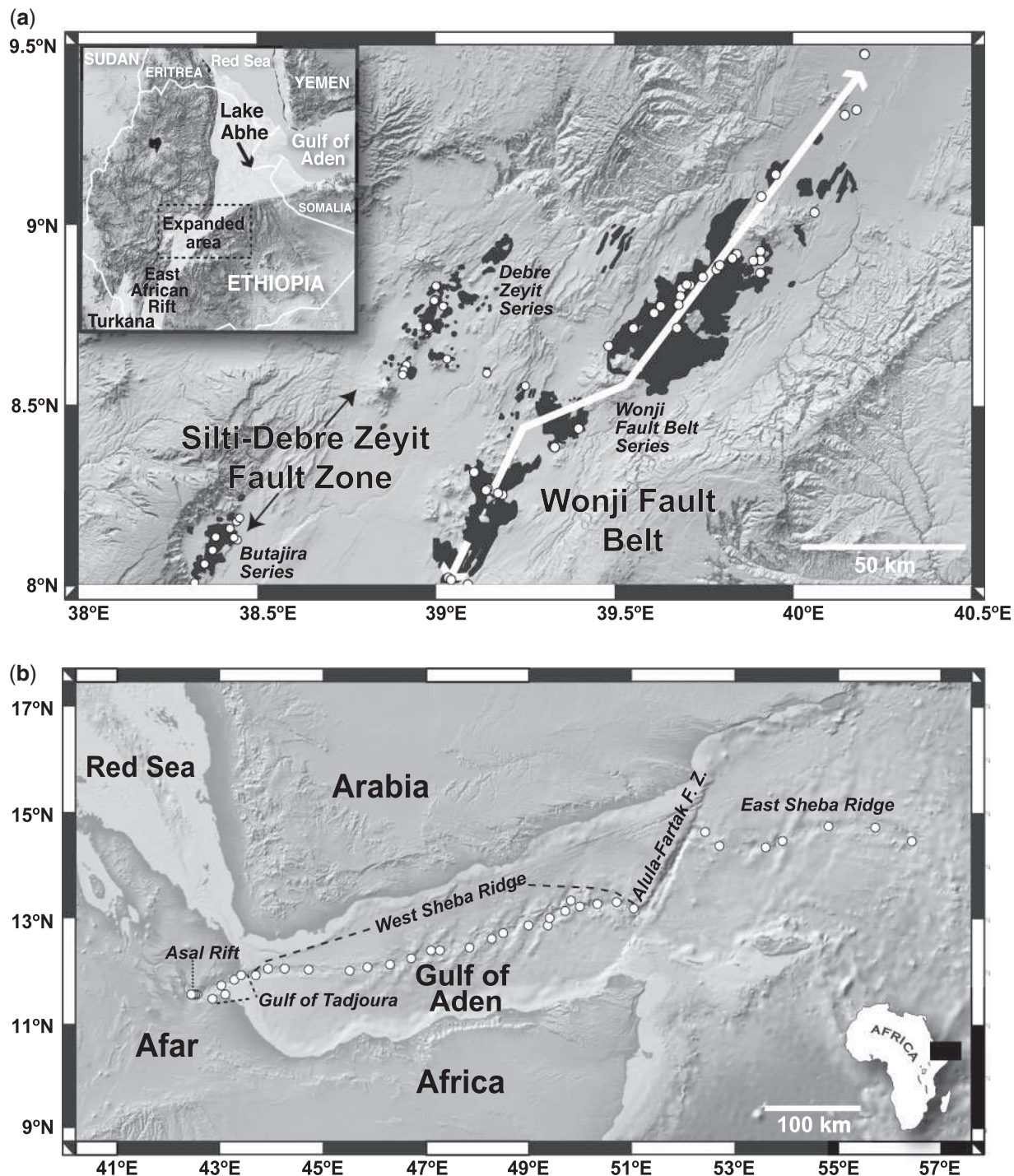
Fig. 1. (a) Map of the Main Ethiopian Rift study area with Quaternary sample locations shown along the Wonji Fault Belt, Debre Zeyit, and Butajira extensional zones. The Debre Zeyit, Butajira, and Wonji Fault Belt zones contain widely (20–40 km) spaced felsic volcanoes and calderas. Samples are from smaller basaltic cinder cones, associated flows, and occasional fissure eruptions that are interspersed between these volcanoes. The inset shows the study area location relative to the Afar triple junction. (b) Map of the Gulf of Aden showing the sample locations of Schilling *et al.* (1992). Backgrounds are reflectance images of East Africa and Yemen from the NASA/JPL Shuttle Radar Tomography Mission (USGS, 2004). The topography and bathymetry are derived from Geomapapp (http://www.geomapapp.org; Ryan *et al.*, 2009).

Table 1: Location and isotope data for basalts from the Main Ethiopian Rift

Location	Lat. (°N)	Long. (°E)	Distance* (km)	$^{206}Pb/^{204}Pb$	$2\sigma\sqrt{n}$	$^{207}Pb/^{204}Pb$	$2\sigma\sqrt{n}$	$^{208}Pb/^{204}Pb$	$2\sigma\sqrt{n}$	$^{87}Sr/^{86}Sr$	$2\sigma\sqrt{n}$	$^{143}Nd/^{144}Nd$	$2\sigma\sqrt{n}$	ε_{Nd}	$^{176}Hf/^{177}Hf$	$2\sigma\sqrt{n}$	ε_{Hf}
Debre Zeyit																	
DZ-1003	8·84	39·00	377	18·1518	6	15·5978	7	38·3801	19	0·704539	2†	0·512631	6	−0·1	0·282839	6	2·4
DZ-1004	8·80	39·00	380	18·5096	10	15·5891	10	38·6038	27	0·703833	14	0·512794	7	3·0			
DZ-1005	8·80	39·00	380	18·3151	10	15·5782	9	38·4726	19	0·703905	8†	0·512763	7	2·4			
DZ-1007	8·72	38·99	388	18·4088	7	15·5723	5	38·5149	13	0·703909	5†	0·512784	7	2·8	0·282997	4	8·0
DZ-1008	8·72	38·98	387	18·4949	9	15·5716	7	38·5552	21	0·703810	2†	0·512808	8	3·3	0·283019	3	8·7
DZ-1009	8·59	39·15	386	18·5007	8	15·5735	7	38·5330	17	0·704173	7†	0·512805	6	3·3	0·283039	4	9·4
DZ-1013	8·62	38·92	401	18·3893	6	15·5742	6	38·4825	18	0·703978	7†	0·512775	8	2·7			
DZ-1014	8·60	38·91	402	18·5816	8	15·5714	7	38·6030	17	0·703825	1†	0·512850	6	4·1	0·283027	4	9·0
Butajira																	
BJ-1053	8·19	38·45	470	18·5166	6	15·5594	5	38·4494	12	0·703652	17	0·512803	9	3·2			
BJ-1051	8·16	38·43	475	18·4916	9	15·5519	8	38·4200	19	0·703631	10	0·512839	6†	3·9	0·283007	4	8·3
BJ-1043	8·14	38·44	476	18·4300	12	15·5519	11	38·3816	28	0·703719	8	0·512804	7	3·2	0·282993	5	7·8
BJ-1049	8·14	38·39	480	18·2712	9	15·5433	8	38·1914	20	0·703582	8	0·512790	6	3·0			
BJ-1044	8·10	38·38	483	18·5186	7	15·5534	6	38·4340	13	0·703647	11	0·512837	6	3·9	0·282997	4	8·0
BJ-1045	8·06	38·36	488	18·5223	7	15·5602	6	38·4697	16	0·703606	14	0·512820	7†	3·6	0·282973	4	7·1
BJ-1048	8·00	38·33	495	18·1741	10	15·5389	13	38·1730	22	0·703786	15	0·512808	7	3·3			
Wonji Fault Belt‡																	
WFB-1026	9·48	40·20	238	18·9194	6	15·5803	5	38·8592	13	0·703681	9†	0·512896	6	5·0			
WFB-1023	9·14	39·95	284	*18·7524*	5	*15·5837*	4	*38·7819*	11	*0·704102*		*0·512845*	7	4·0	0·283049	3	9·8
WFB-1027	9·48	40·20	238	*18·8272*	3	*15·5807*	4	*38·8958*	7	*0·703722*		*0·512890*	28	4·9	0·283075	4	10·7
WFB-E99-2	8·91	39·82	313	18·6022	12	15·5854	13	38·7011	25	*0·704117*		*0·512826*		3·7			
WFB-N-18	8·91	39·83	313	*18·7317*	6	*15·5969*	6	*38·8345*	17	*0·703961*		*0·512827*		3·7	0·283019	4	8·7
WFB-1037	8·86	39·75	323	*18·5571*	4	*15·5840*	4	*38·6318*	9	*0·704251*		*0·512796*	13	3·1	0·283009	5	8·4
WFB-KO-12	8·82	39·68	330	*18·6577*	10	*15·5934*	8	*38·8260*	23	*0·704303*		*0·512793*		3·0			
WFB-KO-4B	8·82	39·68	330	*18·8011*	6	*15·5960*	5	*38·8717*	17	*0·704015*		*0·512829*		3·7			
WFB-N-20	8·83	39·69	329	*18·8109*	6	*15·5923*	5	*38·8730*	17	*0·703996*							
WFB-1035	8·80	39·68	332	*18·6267*	4	*15·5847*	4	*38·7497*	8	*0·704198*		*0·512795*	16	3·1	0·283007	5	8·3
WFB-N-22	8·72	39·68	340	*18·9449*	14	*15·5948*	16	*38·8959*	56	*0·703768*		*0·512866*		4·4	0·283056	3	10·0

Table 1: Continued

Location	Lat. (°N)	Long. (°E)	Distance* (km)	^{206}Pb/^{204}Pb	2σ√n	^{207}Pb/^{204}Pb	2σ√n	^{208}Pb/^{204}Pb	2σ√n	^{87}Sr/^{86}Sr	2σ√n	^{143}Nd/^{144}Nd	2σ√n	ε$_{Nd}$	^{176}Hf/^{177}Hf	2σ√n	ε$_{Hf}$
WFB-N-15	8·78	39·63	337	18·6799	6	15·5883	5	38·8788	15	0·704203		0·512828		3·7			
WFB-1036	8·84	39·71	327	18·8083	4	15·5896	4	38·8616	10	0·703949		0·512827	8	3·7	0·283008	5	8·4
WFB-N-21	8·78	39·68	334	18·6241	12	15·5856	12	38·7938	36	0·704228		0·512821		3·6	0·283009	4	8·4
WFB-E99-20	8·38	39·33	393	18·6940	9	15·5908	7	38·7907	20	0·704117							
WFB-N-01	8·39	39·33	392	18·5185	4	15·5892	4	38·6860	15	0·704485		0·512758		2·3	0·282976	4	7·2
Mojo																	
1010	8·56	39·23	384	17·8821	8	15·5875	8	38·2677	17	0·705289	5†	0·512551	6	−1·7			

*Radial distance from Lake Abhe, Afar (11·25°N, 41·42°E).

Prior to dissolution rock chips were cleaned with distilled 2 N HCl, 1 N HBr, and ultrapure H_2O. Sr, Nd, and Pb were separated for analysis following the procedures of Hanan & Schilling (1989) and Blichert-Toft *et al*. (1997) for Hf. Sr isotopes were measured on a VG Sector 54, seven-collector thermal ionization mass spectrometer in multi-dynamic mode. Hf, Nd, and Pb were analyzed on a Nu Plasma HR multi-collector inductively coupled plasma mass spectrometry (MC-ICP-MS) system using a Nu Instruments desolvating nebulizer equipped with a 100 μl min^{-1} nebulizer (DSN100). The ^{87}Sr/^{86}Sr isotope ratios were normalized to ^{88}Sr/^{86}Sr = 0·1194 to correct for mass fractionation, and the Sr isotopic data are reported relative to NIST SRM 987 = 0·710250. The Nd and Hf isotope ratios were corrected for instrumental mass fractionation and machine bias by applying a discrimination factor determined by bracketing sample runs with analyses of the SDSU AMES Nd standard using a value of 0·512130 and the JMC 475 standard (every two or three samples) with ^{176}Hf/^{177}Hf of 0·282160. Hf isotope sample data are normalized to ^{179}Hf/^{177}Hf = 0·7325 and reported relative to JMC 475 = 0·282160. The CHUR value for ^{176}Hf/^{177}Hf of 0·282772 of Blichert-Toft & Albarède (1997) was used to calculate the ε$_{Hf}$ values. Sample data were normalized to ^{146}Nd/^{144}Nd = 0·7219 and are reported relative to the laboratory value of ^{143}Nd/^{144}Nd = 0·512130 for the SDSU AMES Nd standard. The measured value of La Jolla Nd at SDSU = 0·511844. Pb was separated on two anion exchange columns, a 500 μl followed by a 200 μl column to maximize the Pb separation for optimum ICP-MS analyses. The lead yields were determined to be ~100%, therefore the columns do not have a fractionation effect. The in-run mass discrimination for Pb was determined with NIST SRM 997 Tl with ^{205}Tl/^{203}Tl = 2·3889 and NIST SRM 981 (Todt, 1996) using the method of White *et al*. (2000). The Pb isotope ratios were corrected for machine bias and drift by bracketing the sample analyses with analyses of the NIST SRM 981 (every two samples) corrected for fractionation. Total procedural blanks were: <25 pg Hf, <90 pg Pb, <200 pg Nd, <250 pg Sr. No blank corrections were applied to the data because they are insignificant. The reported uncertainties are 2 standard errors of the mean (2σ√n) for the in-run precision, except for some Nd and Sr samples (†), where the uncertainties represent 2σ√n for 2–3 replicate analyses, and thus provide a measure of sample reproducibility. The NIST SRM 987 standard averaged ^{87}Sr/^{86}Sr = 0·710257 ± 8 2σ√n, n = 16, AMES Nd standard averaged ^{143}Nd/^{144}Nd = 0·512118 ± 2 2σ√n, n = 22, JMC475 standard averaged 0·282151 ± 0·000001 2σ√n, n = 21, and NIST SRM 981 averaged ^{206}Pb/^{204}Pb = 16·9361 ± 0·0004, ^{207}Pb/^{204}Pb = 15·4914 ± 0·0004, ^{208}Pb/^{204}Pb = 38·6981 ± 0·0012 2σ√n, n = 17.

‡The analyses in italics for the Wonji Fault Belt were published previously (Furman *et al*., 2006). The Pb isotopes for the Furman *et al*. (2006) Wonji Fault Belt data were analyzed at SDSU under the same conditions as reported here. We have added the fourth decimal place and errors (from the SDSU data archives) to be consistent with the new Main Ethiopian Rift data. The analytical methods and procedures for Nd and Sr have been reported by Furman *et al*. (2006). The Nd isotope ratios for these samples have been renormalized to the SDSU La Jolla = 0·511844 and the Sr isotope ratios are normalized to NIST SRM 987 = 0·710250.

Table 2: Location and Hf isotope data for the Gulf of Aden basalts

Sample	Latitude (°N)	Longitude (°E)	Distance* (km)	^{176}Hf/ ^{177}Hf	$2\sigma\sqrt{n}$	ε_{Hf}
Asal Rift						
DJ-74	11·60	42·48	122	0·283122	6	12·4
DJ-42	11·60	42·49	122	0·283161	7	13·8
DJ-26	11·60	42·50	123	0·283130	5	12·7
DJ-18	11·60	42·51	124	0·283115	5	12·1
DJ-9	11·60	42·51	125	0·283141	4	13·0
DJ-5	11·60	42·52	126	0·283144	5	13·2
DJ-2	11·60	42·52	126	0·283141	4	13·0
Gulf of Tadjoura						
VD-11	11·51	42·85	158	0·283070	5	10·5
V-60 g	11·75	43·02	183	0·283077	6	10·8
VD-39	11·59	43·10	187	0·283122	10	12·4
V-55	11·87	43·27	213	0·283083	5	11·0
V3307 41D-1	11·94	43·41	229	0·283098	5	11·5
Tadjoura Trough						
V3307 42D-1 g	11·94	43·69	259	0·283134	5	12·8
V3307 44D-2 g	12·08	43·93	289	0·283263	6	17·4
V3307 46D-1 g	12·06	44·71	370	0·283230	6	16·2
West Sheba Ridge						
V3307 47D-1 g	12·07	44·83	382	0·283186	8	14·6
V3307 48D-2 g	12·04	45·21	422	0·283138	8	12·9
V3307 49D-1	12·04	45·51	454	0·283008	9	8·3
V3307 50D-1 g	12·10	45·85	492	0·283105	7	11·8
V3307 51D-1 g	12·16	46·29	539	0·283126	7	12·5
V3307 52D-1 g	12·27	46·71	587	0·283274	7	17·8
V3307 53D-1	12·42	47·10	632	0·283304	6	18·8
V3307 54D-1 g	12·42	47·25	648	0·283225	5	16·0
V3307 55D-2 g	12·47	47·84	712	0·283270	7	17·6
V3307 56D-1 g	12·65	48·27	762	0·283262	6	17·3
V3306 39D-1 g	12·75	48·49	788	0·283246	5	16·8
V3307 57D-1 g	12·90	48·99	844	0·283284	7	18·1
V3307 58D-1	12·90	49·36	883	0·283309	12	19·0
V3307 59D-1 g	13·04	49·39	890	0·283253	7	17·0
V3307 60D-1	13·16	49·69	925	0·283302	6	18·7
V3307 62D-1 g	13·36	49·81	942	0·283315	7	19·2
V3307 61D-2 g	13·26	49·97	958	0·283277	6	17·9
V3307 63D-3 g	13·29	50·32	995	0·283295	7	18·5
V3307 64D-3 g	13·34	50·69	1036	0·283339	7	20·1
V3307 65D-1 g	13·21	51·02	1068	0·283349	8	20·4
East Sheba Ridge						
V3306 35D-1	14·65	52·41	1254	0·283293	6	18·4
V3307 66D-1 g	14·39	52·68	1275	0·283163	7	13·8
V3307 67D-1 g	14·37	53·58	1368	0·283257	7	17·2

(continued)

Table 2: Continued

Sample	Latitude (°N)	Longitude (°E)	Distance* (km)	^{176}Hf/ ^{177}Hf	$2\sigma\sqrt{n}$	ε_{Hf}
V3306 25D-1	14·48	53·91	1406	0·283134	5	12·8
V3306 24D-1 g	14·75	54·80	1508	0·283187	6	14·7
V3307 68D-1 g	14·74	55·71	1603	0·283189	8	14·7
V3307 69D-1 g	14·47	56·42	1672	0·283201	7	15·2

*Radial distance from Lake Abhe, Afar.
Hf isotope data reported for the Gulf of Aden sample suite were analyzed by MC-ICP-MS (Plasma 54) at the Ecole Normale Supérieure in Lyon following the procedures of Blichert-Toft *et al.* (1997). The JMC-475 Hf standard, which was run every two samples, averaged 0.282160 ± 0.000010 during the analytical run sessions of the Gulf of Aden samples. The total procedural Hf blank was less than 20 pg. The CHUR value for ^{176}Hf/^{177}Hf of 0·282772 of Blichert-Toft and Albarède (1997) was used to calculate the ε_{Hf} values. The Pb, Sr, and Nd isotope compositions have been reported by Schilling *et al.* (1992).

(Rooney *et al.*, 2005, 2007) and the samples fall largely within the range observed globally for mantle-derived basalts (Hofmann *et al.*, 1986, 2005). We also examined the relationship between K/P and Ti/Yb and the Nd and Sr isotope ratios for the Main Ethiopian Rift lavas. Concurrent increases in K/P with increasing ^{87}Sr/^{86}Sr (or decreasing ^{143}Nd/^{144}Nd or ^{176}Hf/^{177}Hf) are indicative of silicic crustal assimilation (Hart *et al.*, 1989). We observed no consistent relationships between Sr, Nd, Hf, or Pb isotope ratios and K/P. The Main Ethiopian Rift lavas have Ti/Yb ratios of about 6000–10 000 (except for sample 1003, which has Ti/Yb = 4500 and contains mafic crustal xenoliths; Rooney *et al.*, 2005). Low K/P <6·5 accompanied by high Ti/Yb (>6000) for the Main Ethiopian Rift lavas rule out significant crustal contamination (Leeman & Hawkesworth, 1986; Van Calsteren *et al.*, 1986; Hart *et al.*, 1989). Furthermore, the He isotope data presented below show that the signature of the Afar plume, as well as the upper mantle, dominates the He isotope variations in the Main Ethiopian Rift basalts selected for this study, which indicates that any potential crustal contamination is minor. The lack of crustal assimilation in these magma suites is consistent with focused recent volcanism in the Wonji Fault Belt and Silti-Debre Zeyit Fault Zone (e.g. WoldeGabriel *et al.*, 1990; Ebinger & Casey, 2001; Casey *et al.*, 2006). Magmas have re-utilized earlier conduits, incorporating xenocrysts and cumulate xenoliths from the walls, with apparently little interaction with the continental lithosphere on their way to the surface (Rooney *et al.*, 2005).

Table 3: Location and He isotope data for basalts from the Main Ethiopian Rift

| Sample	Lat. (°N)	Long. (°N)	Distance (km)	Phase	Wt (mg)	^{3}He/^{4}He R/R$_A$	$2\sigma\sqrt{n}$	[He]
Debre Zeyit								
DZ-1014	8·60	38·91	402	cpx	598·1	5·61	0·34	1·66E – 09
DZ-1009	8·59	39·15	386	olivine	442·1	8·30	0·40	2·59E – 09
DZ-1007	8·72	38·99	388	olivine	744·6	8·66	0·14	1·12E – 08
DZ-1008	8·72	38·98	387	olivine	581·5	8·80	0·16	1·06E – 08
Butajira								
BJ-1045	8·06	38·36	488	olivine	422·4	7·52	0·30	4·22E – 09
BJ-1045	8·06	38·36	488	cpx	420·0	7·53	0·16	1·14E – 08
BJ-1053	8·19	38·45	470	cpx	541·4	7·70	0·24	4·91E – 09
BJ-1043	8·14	38·44	476	olivine	430·4	8·11	0·36	2·55E – 09
Wonji Fault Belt								
WFB-1027	9·48	40·20	238	olivine	428·6	12·66	0·98	7·49E – 10
WFB-1036	8·84	39·71	327	olivine	631·4	12·16	0·24	8·02E – 09
WFB-N-21	8·78	39·68	334	olivine	537·8	12·82	0·26	6·40E – 09
WFB-N-14	8·76	39·61	340	olivine	871·4	15·12	0·30	3·13E – 09

Helium isotope analyses were carried out by *in vacuo* crushing of mineral separates from the Ethiopian basalts. Analytical procedures have been described elsewhere (Graham *et al.*, 1998). The reported uncertainties are 2 standard errors, computed from the quadrature sum of uncertainties associated with the sample analysis, air standard analyses and blank determinations. Distance is measured radially in kilometers.

Isotope signatures, mantle components, and mixing

The isotopes of Pb, Sr, Nd, Hf, and He are powerful tracers of mantle dynamics, because mantle-derived basalts fall into distinct subdivisions based on their radiogenic isotope compositions (White & Hofmann, 1982; Zindler & Hart, 1986; Hofmann, 1997). These subdivisions are related to distinct processes (pelagic vs terrigenous sediment subduction, hydrothermal alteration, etc.) as well as to distinct tectonic or petrogenetic environments (e.g. mid-ocean ridge, oceanic plateau, island arc, etc.). As one example, DUPAL signatures (Hart, 1984) may arise from the recycling of oceanic and/or continental lithosphere, ranging from ancient (EM I) to recent (EM II) in age, may be associated with, respectively, ancient and recent sediments, and may include metasomatized lithosphere (e.g. HIMU) (Zindler & Hart, 1986; Mahoney *et al.*, 1989, 1992, 1996; McKenzie & O'Nions, 1995; Rehkämper & Hofmann, 1997; Lustrino, 2005; Willbold & Stracke, 2010). The source of MORB is best constrained in terms of its location in the mantle, and corresponds to the trace-element depleted upper mantle MORB source (White & Hofmann, 1982; Zindler & Hart, 1986). The common isotopic component C, defined by the convergence of trends in Pb isotope compositional space (at relatively radiogenic Pb; ^{206}Pb/^{204}Pb $= 19·6 \pm 0·4$) for MORB from the Atlantic,

Pacific and Indian Oceans, has been attributed to the presence of recycled oceanic lithosphere in the mantle source region of many MORB (Hanan & Graham, 1996). In contrast, the mantle component FOZO, defined by the convergence of global ocean island basalt isotopic trends, has been attributed to the presence of deep, relatively primitive mantle (Hart *et al.*, 1992; Hauri *et al.*, 1994), although this interpretation has since been modified (Stracke *et al.*, 2005). Mixing models involving these mantle components and end-members, however, often cannot define a unique source for the basalts. In particular, for continental rift basalts it is difficult to distinguish a deep mantle component derived by melting recycled lithosphere from shallower melting involving old subcontinental lithosphere. Although this is a challenging problem, the systematics of mixing during petrogenesis can be deciphered using a multi-isotopic approach. For example, the order of mixing between three end-members may be revealed through the combined use of ^{208}Pb–^{207}Pb–^{206}Pb isotopes (Hanan *et al.*, 1986; Hanan & Schilling, 1997; Douglass & Schilling, 2000). Systematic spatial and temporal variations in this isotope space provide further constraints on the mixing sequence. Mixing models typically use exactly chosen values for end-member compositions to avoid the mathematical complexity that arises from the mixing of heterogeneous end-members. However, mantle sources
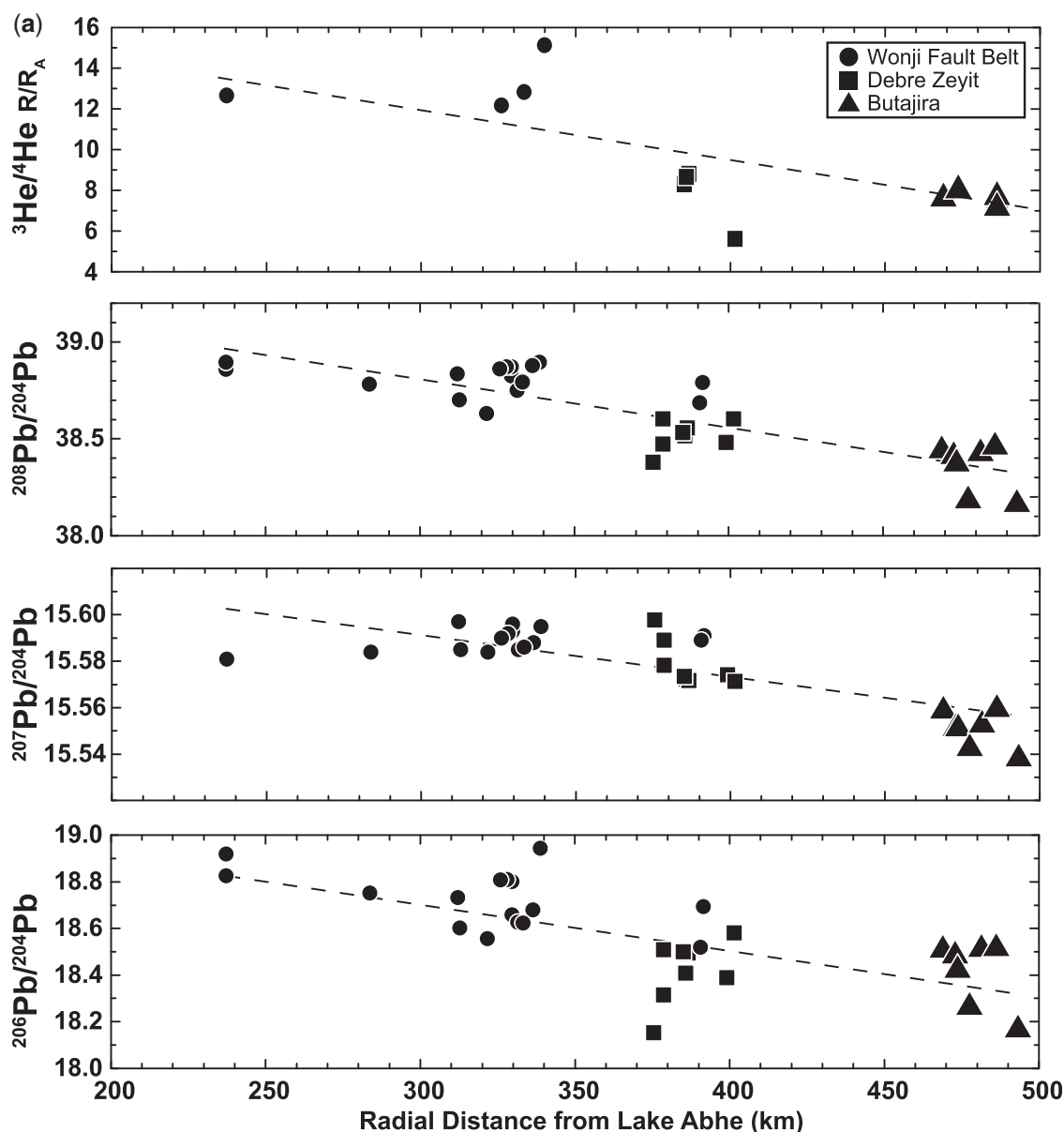
Fig. 2. (a) Variation of $^{206}Pb/^{204}Pb$ ($r^2 = 0.48$), $^{207}Pb/^{204}Pb$ ($r^2 = 0.60$), $^{208}Pb/^{204}Pb$ ($r^2 = 0.83$), and $^3He/^4He$ R/R_A ($r^2 = 0.53$), and (b) $^{87}Sr/^{86}Sr$, ε_{Nd}, and ε_{Hf} in Quaternary lavas of the Main Ethiopian Rift (Wonji Fault Belt, Debre Zeyit, and Butajira) as a function of radial distance from the inferred present-day location of the Afar plume axis in the Lake Abhe region (Table 1). (c) Variation of $^{87}Sr/^{86}Sr$ ($r^2 = 0.18$), ε_{Hf} ($r^2 = 0.14$), ε_{Nd} ($r^2 = 0.10$), and $^{206}Pb/^{204}Pb$ ($r^2 = 0.036$) as a function of radial distance from the Afar plume center for the Asal Rift, Gulf of Tadjoura, Tadjoura Trough and the Sheba Ridge. The prominent shift in ε_{Hf} across the Alula-Fartak fracture zone as the East Sheba Ridge steps northward towards Yemen should be noted. The trend lines [in (a) and (c); dashed black lines] represent the least-squares linear regression for the Main Ethiopian Rift [from (a) and (b)]. The 'by eye' trends for the Gulf of Aden data are shown by a thin dashed line in (c). The Gulf of Aden Hf isotope data are from Table 2 and the Pb, Sr, and Nd isotope data are from Schilling *et al.* (1992). Also shown are the Main Ethiopian Rift data from (a) and (b) and Table 1. Negative distances signify samples from along the Gulf of Aden, positive distances indicate samples along the East African Rift. E- and W-Torus refer to the position of the torus plume head beneath the Main Ethiopian Rift and Gulf of Aden as proposed by Schilling *et al.* (1992). Debre Zeyit sample DZ-1003 is labeled.

are, by their very nature, heterogeneous to varying degrees, and, hence, simple mixing models assuming homogeneous end-members should be viewed only as approximations; they cannot be expected to account for all the natural variability observed in most sample suites.

The approach that we adopt below also involves a multi-component mixing model with fixed end-member compositions. Nevertheless, we impose rigorous mathematical and statistical tests to evaluate the ability of the model to account for the observed geochemical variability
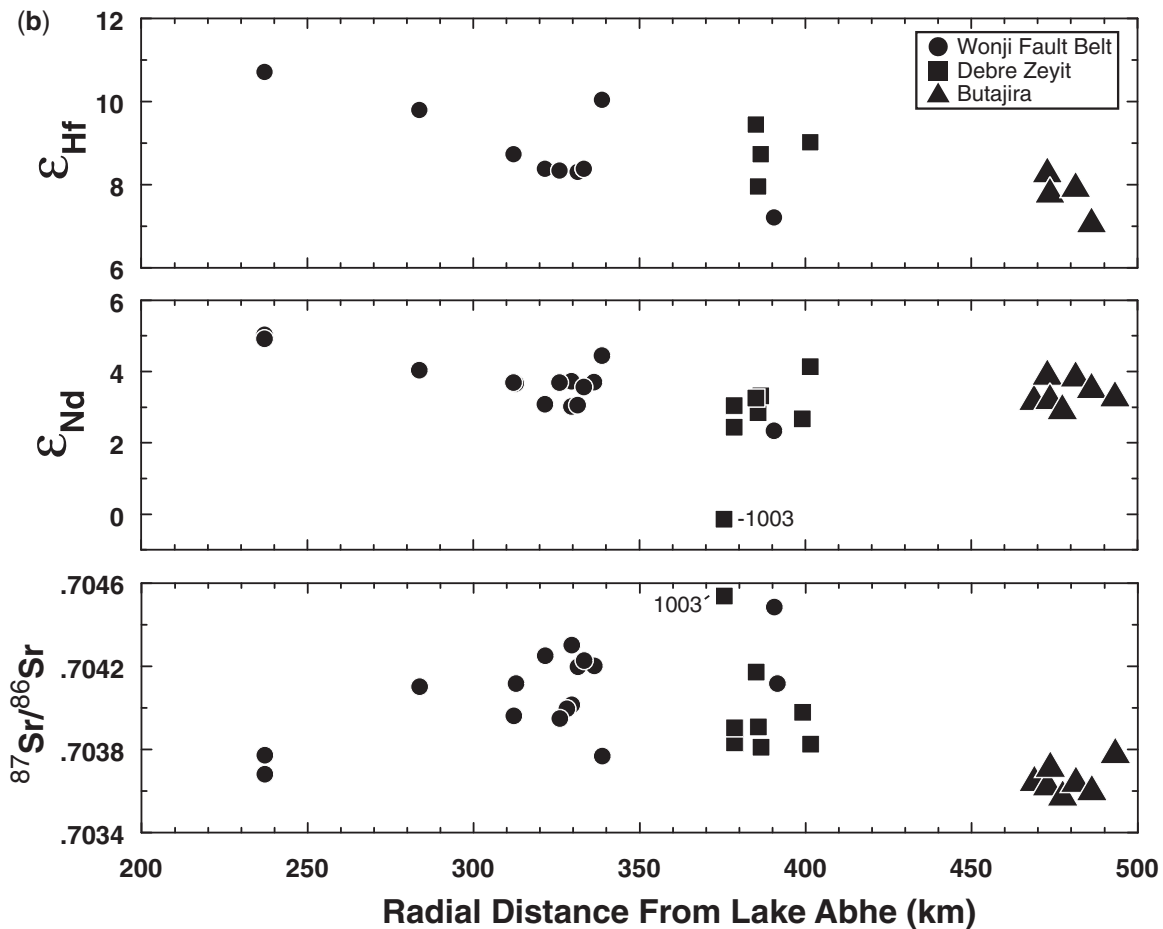
Fig. 2. Continued.

in the Main Ethiopian Rift sample suite. The details and mathematical development of this multi-component mixing model are well documented (e.g. Hanan *et al.*, 1986, 2000; Schilling *et al.*, 1992; Hanan & Schilling, 1997; Douglass & Schilling, 2000), and its algorithms and rationale have been given by Schilling *et al.* (1992), Albarède (1995) and Douglass & Schilling (2000) and hence are not repeated here.

RESULTS
Pb–Sr–Nd–Hf–He spatial isotope variations

The Pb–Sr–Nd–Hf–He isotope variations along the axis of the Main Ethiopian Rift, relative to the presumed location of the center of the Afar plume beneath the Lake Abhe region, are shown in Fig. 2a and b. The location of the plume center near Lake Abhe is based on a synthesis of independent structural, tectonic, magnetic, and geochemical data that all focus toward this region (Schilling, 1973*b*). The new Pb, Sr, Nd, and Hf isotope ratios for the Main

Ethiopian Rift lavas all become more radiogenic upon approaching the inferred plume center, except for $^{87}Sr/^{86}Sr$ and $^{207}Pb/^{204}Pb$ in two Wonji Fault Belt samples closest to the plume, which appear to be slightly low (Table 1; Fig. 2). In addition, $^{143}Nd/^{144}Nd$ and $^{176}Hf/^{177}Hf$ data for Butajira basalts are not quite as low as predicted by a monotonic linear trend (Fig. 2b). There is a general trend of increasing $^3He/^4He$ towards Lake Abhe (Table 3). However, there is also significant variation on a shorter length scale; for example, the highest $^3He/^4He$ in our sample suite (15·1 R_A) occurs in a Wonji Fault Belt lava at ~340 km distance (sample WFB N-14), similar to what is observed for $^{206}Pb/^{204}Pb$ (Fig. 2a). The bulk composition of sample N-14, which contains abundant plagioclase and olivine phenocrysts relative to the other samples, is unlikely to represent a magmatic liquid because it falls off the major element trends of the combined dataset (e.g. CaO/Al_2O_3 and MgO).

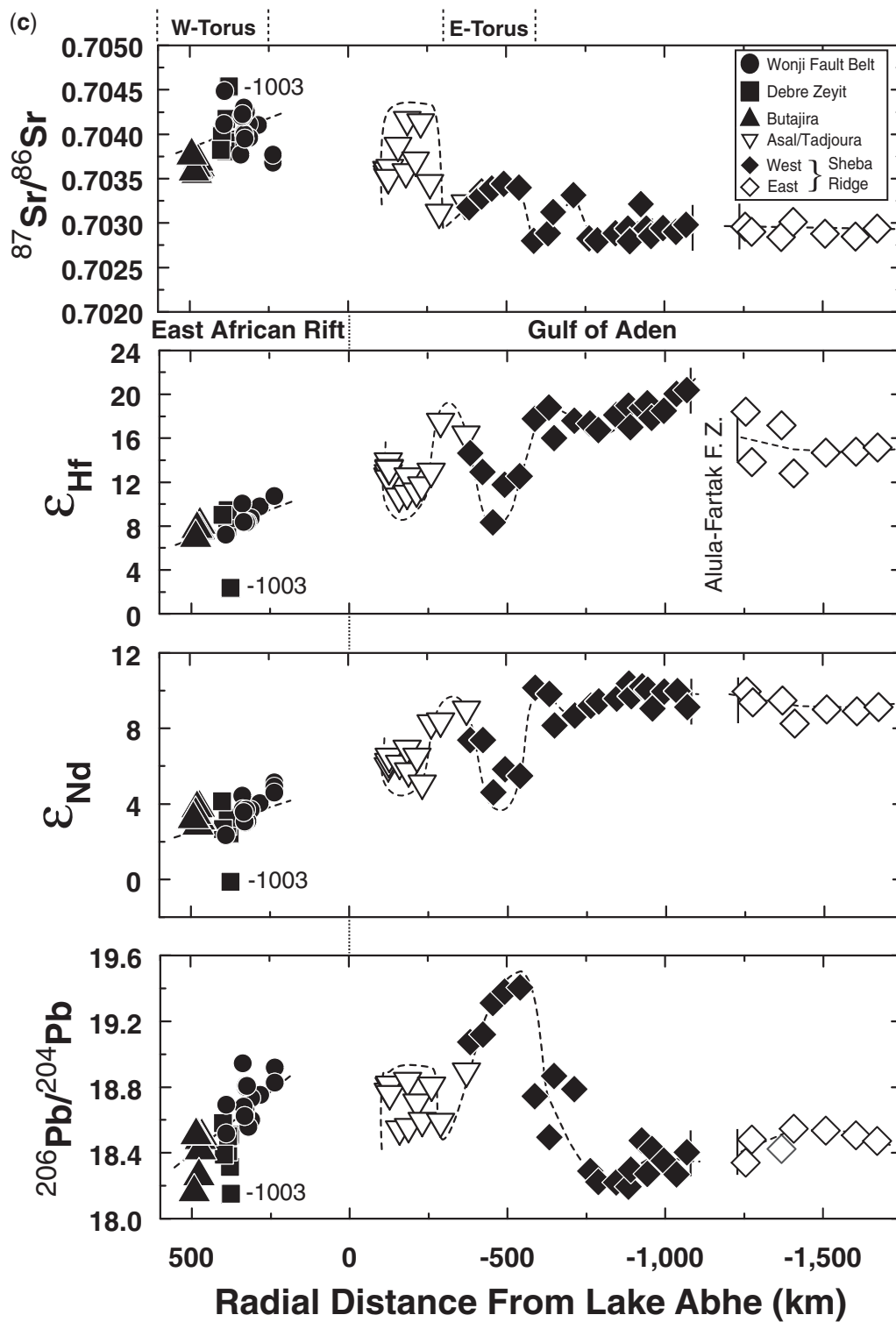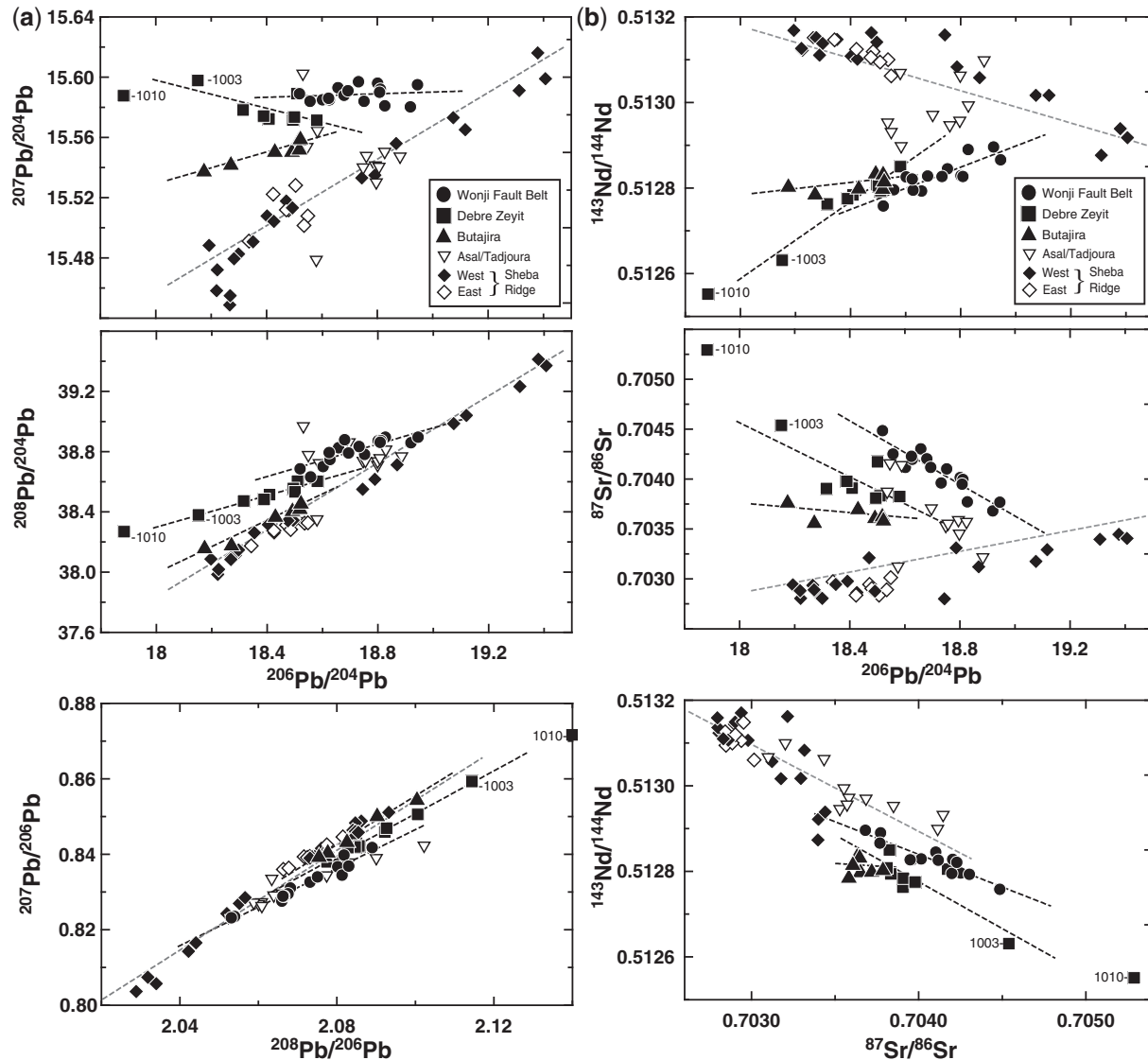The similar profiles for Pb, Sr, Nd, Hf, and He isotopes are not expected, because mantle-derived lavas

Fig. 2. Continued.

Fig. 3. (a) Covariation of $^{208}Pb/^{204}Pb$ and $^{207}Pb/^{204}Pb$ with $^{206}Pb/^{204}Pb$, and $^{207}Pb/^{206}Pb$ with $^{208}Pb/^{206}Pb$ in the Main Ethiopian Rift Quaternary and Gulf of Aden sample suites. The dashed lines are least-squares regression lines for the Gulf of Aden, Wonji Fault Belt, Debre Zeyit, and Butajira volcanic zones. (b) Covariation of $^{143}Nd/^{144}Nd$ and $^{87}Sr/^{86}Sr$ with $^{206}Pb/^{204}Pb$, and $^{143}Nd/^{144}Nd$ with $^{87}Sr/^{86}Sr$ in the Wonji Fault Belt, Debre Zeyit, and Butajira volcanic zones and Gulf of Aden sample suites. The dashed lines represent the least-squares linear regression lines of the datasets for the Main Ethiopian Rift and Gulf of Aden data. Debre Zeyit samples Mojo l0l0 and DZ-l003 are labeled.

usually show broad anti-correlation between $^{143}Nd/^{144}Nd$ (or $^{176}Hf/^{177}Hf$) and $^{87}Sr/^{86}Sr$ (or $^{206}Pb/^{204}Pb$) reflecting long-term *in situ* radiogenic production. The signatures observed here, therefore, rather reflect recent mixing.

The variations in Nd–Sr–Pb–Hf isotope compositions and La/Sm ratios along the Gulf of Aden spreading center define an 800 km long gradient eastward from the Afar region, based on samples from the Asal Rift, Gulf of Tadjoura, Tadjoura Trough, and along the Sheba Ridge to about 50°E (Schilling *et al.*, 1992; Table 2). The Asal Rift and Gulf of Tadjoura represent a nascent stage of rift evolution, characterized by diffuse extension. In contrast, the more developed Sheba Ridge is approaching steady-state seafloor spreading. The differences in the rift development stage are reflected in the Pb, Sr, Nd, and Hf isotope characteristics of the basalts. The West Sheba Ridge shows an enrichment peak for Pb, Sr, Nd, and Hf isotopes and large ion lithophile elements (LILE) centered around 46°E, about 500 km east of the presumed plume center (Table 2). East of 48°E, Pb, Sr, Nd, and Hf isotope compositions show much less variation. The $^{206}Pb/^{204}Pb$, $^{87}Sr/^{86}Sr$, ε_{Nd}, and ε_{Hf} display similar spatial variation

(Fig. 2c) consisting of well-defined alternating peaks and troughs. Although the peaks and troughs appear to be slightly out of phase, there is no apparent fracture zone control on the Pb, Sr, and Nd isotope compositions (Fig. 2; Schilling *et al.*, 1992). However, the new Hf isotope data show a step at the Alula-Fartak fracture zone toward less radiogenic, more continental-like signatures, as the ridge jumps northeastward toward Yemen. The Asal Rift and Gulf of Tadjoura show a much smaller enrichment spike in Pb, Nd, and Hf isotope ratios relative to the Sheba Ridge. However, ^{206}Pb/^{204}Pb is more radiogenic, ε_{Nd} and ε_{Hf} are less radiogenic than observed in the LILE-depleted basalts of the East Sheba Ridge and all overlap the range of the West Sheba Ridge samples. The range in ^{87}Sr/^{86}Sr for the Asal Rift and Gulf of Tadjoura data is distinctly higher than observed along the entire Sheba Ridge. The anomaly at 46°E was previously attributed to the interaction of the Sheba Ridge with a torus-like mantle plume (Schilling *et al.*, 1992). In the torus plume model, the Gulf of Tadjoura and Asal Rift overlie a mantle region located to the inside of a plume-head torus, where the mantle source is proposed to be dominated by Pan-African continental lithosphere and the upper mantle asthenosphere (Fig. 2c; Schilling *et al.*, 1992). The plume torus overlies the enrichment peaks in radiogenic Pb and Sr and corresponding troughs in ε_{Nd} and ε_{Hf} located on the Sheba Ridge at about 500 km from the plume center. In the Schilling *et al.* (1992) model, the opposite side of the torus would be located at a similar distance from the plume center, along the southwestern Main Ethiopian Rift.

Pb–Pb isotope correlations

The new data for the Main Ethiopian Rift were collected from three spatially resolvable sections of the Main Ethiopian Rift: Debre Zeyit, Butajira, and the Wonji Fault Belt. The Debre Zeyit and Butajira volcanic fields are two major zones of volcanism and tectonism separated by a 50 km gap that comprises the northernmost portion of the Silti-Debre Zeyit Fault Zone (WoldeGabriel *et al.*, 1990; Rooney *et al.*, 2011). The most distinctive Quaternary magmatic feature in the Ethiopian Rift is the Wonji Fault Belt, which extends from around Lake Abhe into southern Ethiopia (Mohr, 1967). The three sample populations (Debre Zeyit, Butajira, and Wonji Fault Belt) have different, but overlapping ranges in Pb isotope ratios, and appear to form distinct arrays in Pb–Sr–Nd–Hf multi-isotope space (Figs 3a, b and 4; Table 4). This raises the question of whether the three spatially distinct datasets can be treated as a single population, or whether they constitute three distinct sub-populations.

Least-squares linear regressions of the three datasets show that their trends are significantly different at the 95% confidence level for both the ^{206}Pb/^{204}Pb vs ^{208}Pb/^{204}Pb and ^{207}Pb/^{204}Pb binary projections (Table 4).

The three sub-populations (Wonji Fault Belt, Debre Zeyit, and Butajira) define linear arrays in Pb isotopic space, with r^2 values of 0·68, 0·93, and 0·97, respectively, in the ^{208}Pb/^{204}Pb vs ^{206}Pb/^{204}Pb diagram (Fig. 3a). In the ^{207}Pb/^{204}Pb vs ^{206}Pb/^{204}Pb diagram the trends for Debre Zeyit and Butajira have r^2 values of 0·43 and 0·89, respectively. The Wonji Fault Belt data form a near horizontal array with $r^2 = 0·02$. The r^2 statistic measures how significantly the slope of a fitted line differs from zero, and is not necessarily a measure of good fit. To further test the validity of subdividing the data on the basis of spatial location, we performed analysis of the covariance of the Pb–Pb least-squares regression lines for each of the sub-populations against the combined datasets of the other two areas. The rationale for this comparison is that if all the data fall along the same regression, then removing a subset of the data should not affect the pooled regression. We tested the null hypothesis that the least-squares regression for a sub-population was the same as the regression for the other two groups combined. The *F*-test results for ^{208}Pb/^{204}Pb and ^{207}Pb/^{204}Pb vs ^{206}Pb/^{204}Pb, using the slopes and intercepts of the least-squares linear regressions for the three sub-populations (Wonji Fault Belt, Debre Zeyit, and Butajira) relative to the data subsets containing the other two groups, allow rejection of the null hypothesis at the 95% confidence level (Table 5). Therefore, these three sample suites, from spatially different volcanic belts, have distinct Pb isotope correlations, or trends, and define three statistically distinct sub-populations that make up the complete Main Ethiopian Rift sample suite of this study.

Nd–Hf isotope correlations

In ε_{Nd} vs ε_{Hf} isotope space (Fig. 5a) the Main Ethiopian Rift data lie along and above the mantle array, trending between the Afar plume, as represented by the C field, and compositions typical of ancient lithosphere. In contrast, the new data from the Sheba Ridge axis in the Gulf of Aden and its extension into the Gulf of Tadjoura and the Asal Rift plot at more radiogenic values of ε_{Hf} and ε_{Nd}, similar to Indian Ocean MORB with predominantly positive values of $\Delta\varepsilon_{Hf}$, rather than negative $\Delta\varepsilon_{Hf}$ values such as those of most Pacific MORB (Fig. 5; $\Delta\varepsilon_{Hf}$ is the vertical displacement from the mantle array in ε_{Hf} units for a data point in the ε_{Nd} vs ε_{Hf} diagram). Both the Main Ethiopian Rift and the Gulf of Tadjoura–Asal Rift data have distinct high Δ^{208}Pb/^{204}Pb (where Δ^{208}Pb/^{204}Pb is relative to the ^{208}Pb/^{204}Pb of the Sheba Ridge array at any given ^{206}Pb/^{204}Pb; Fig. 3a). These observations are consistent with the different tectonic settings. The Sheba Ridge data reflect an origin dominated by plume–oceanic lithosphere interaction (e.g. Schilling *et al.*, 1992), whereas the Main Ethiopian Rift and the Gulf of Tadjoura–Asal Rift data indicate strong influence from a continental lithosphere component, in line with a continental rift setting.
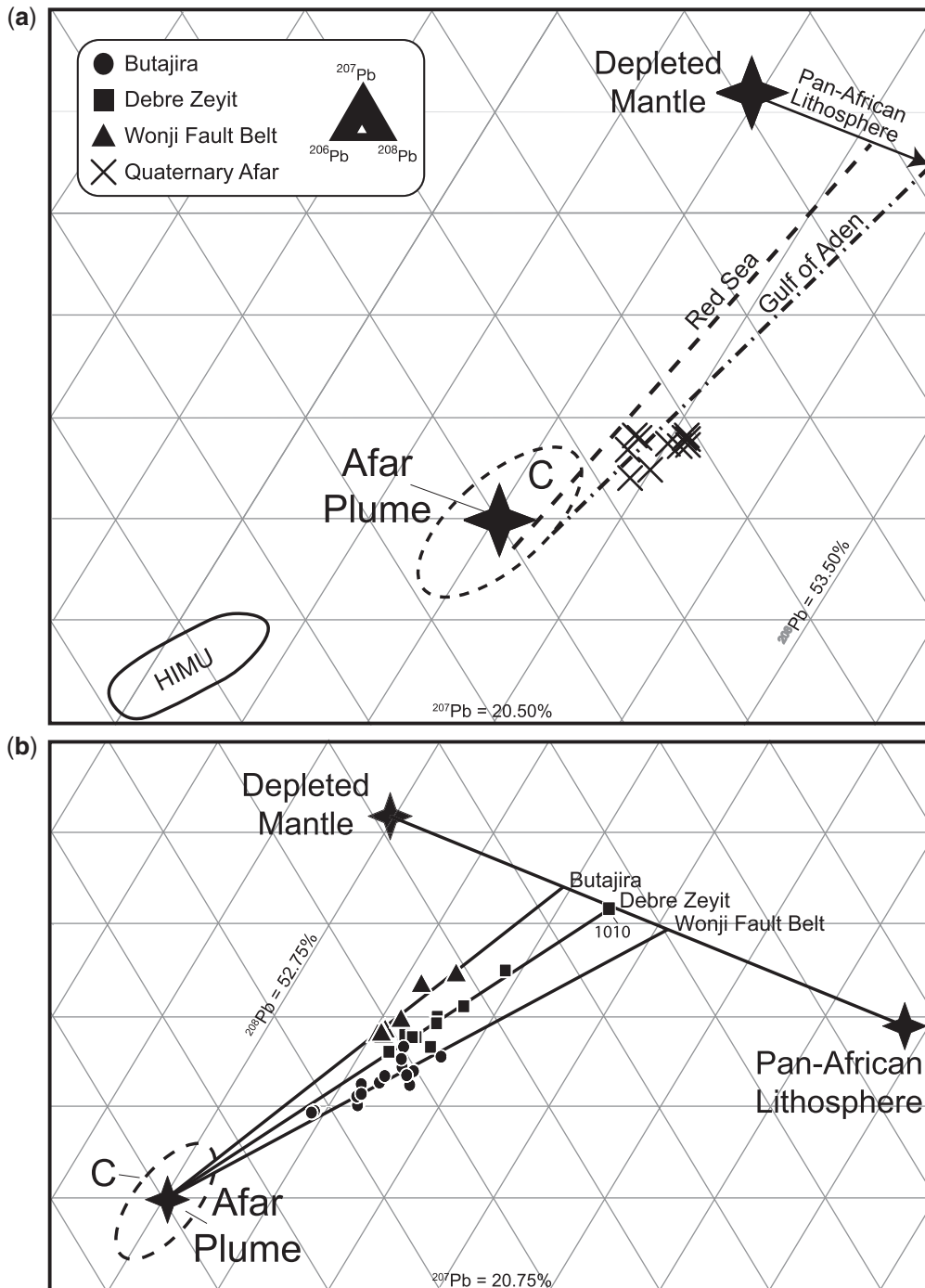
Fig. 4. (a) Triangular Pb isotope plot (after Hanan *et al.*, 1986) of the relative abundances of ^{206}Pb, ^{207}Pb, and ^{208}Pb in Quaternary lavas from Afar and the northern Main Ethiopian Rift (Deniel *et al.*, 1994). Only lavas having MgO > 7 wt % are included, to limit the potential variation related to shallow crustal processes. The least-squares trend for the Red Sea and Gulf of Aden are shown for comparison. Data for the Red Sea are from Altherr *et al.* (1988), Rogers (1993), and Volker *et al.* (1993, 1997), and for the Gulf of Aden from Schilling *et al.* (1992). (b) Triangular Pb isotope plot (after Hanan *et al.*, 1986) of the relative abundances of ^{206}Pb, ^{207}Pb, and ^{208}Pb in lavas from the Main Ethiopian Rift and the model end-members depleted mantle, Pan-African lithosphere, and the Afar plume. Basalts from Butajira, Debre Zeyit, and the Wonji Fault Belt define three distinct pseudo-binary mixing arrays that converge at the composition of the Afar plume, which lies within the range of compositions for the common component 'C' deduced from oceanic basalts (Hanan & Graham, 1996). The depleted ends of the mixing arrays are characterized by three ratios of depleted mantle to Pan-African lithosphere, each of which is constant over the range of mixing seen in the three arrays. The proportion of the Afar plume is largest for the Wonji Fault Belt basalts (~240–440 km from the Afar plume center), smallest for the Butajira basalts (~470–500 km distant), and intermediate for the Debre Zeyit basalts (~370–400 km distant). Sample Mojo-1010 is labeled. The ternary grid is drawn at 0·25% intervals. The ternary grid interval is 0.25%.

Table 4: Characteristics of slopes fitted to the linear arrays in Pb isotope space for Main Ethiopian Rift magmas

Pb isotopes	Region	Test	Value for single belt	Value for other two belts pooled
206–208	WFB	Slope	0·54	0·69
		Intercept	28·75	25·67
	DZ	Slope	0·52	1·12
		Intercept	28·87	17·90
	BJ	Slope	0·88	0·78
		Intercept	22·23	24·25
207–206	WFB	Slope	0·01	0·00
		Intercept	15·49	15·55
	DZ	Slope	−0·05	0·08
		Intercept	16·44	14·12
	BJ	Slope	0·05	0·01
		Intercept	14·58	15·34

Differences between the slopes and intercepts can be utilized to examine differences and similarities between the groups (BJ, Butajira; DZ, Debre Zeyit; WFB, Wonji Fault Belt) using statistical methods (F-test; see Table 5).

Hf–Pb isotope correlations

In ε_{Hf} vs $^{206}Pb/^{204}Pb$ space the West Sheba Ridge array extends between the fields for the most depleted MORB from the Southwest Indian Ridge and the C-like Afar plume. In contrast, the Main Ethiopian Rift data extend between the Pan-African lithosphere and the Afar plume end-member (Fig. 5b). The Asal Rift and Tadjoura data have affinity to, and overlap with, the East Sheba Ridge data in a region of the diagram between the Main Ethiopian Rift and the West Sheba Ridge arrays, displaced toward the Pan-African lithosphere component. Overall, the combined dataset, consisting of the Main Ethiopian Rift and the Gulf of Aden samples, has Indian Ocean-like Hf and Pb isotope signatures, distinct from the Pacific asthenosphere MORB source (Fig. 5c) and consistent with a continental-like mantle source component.

DISCUSSION
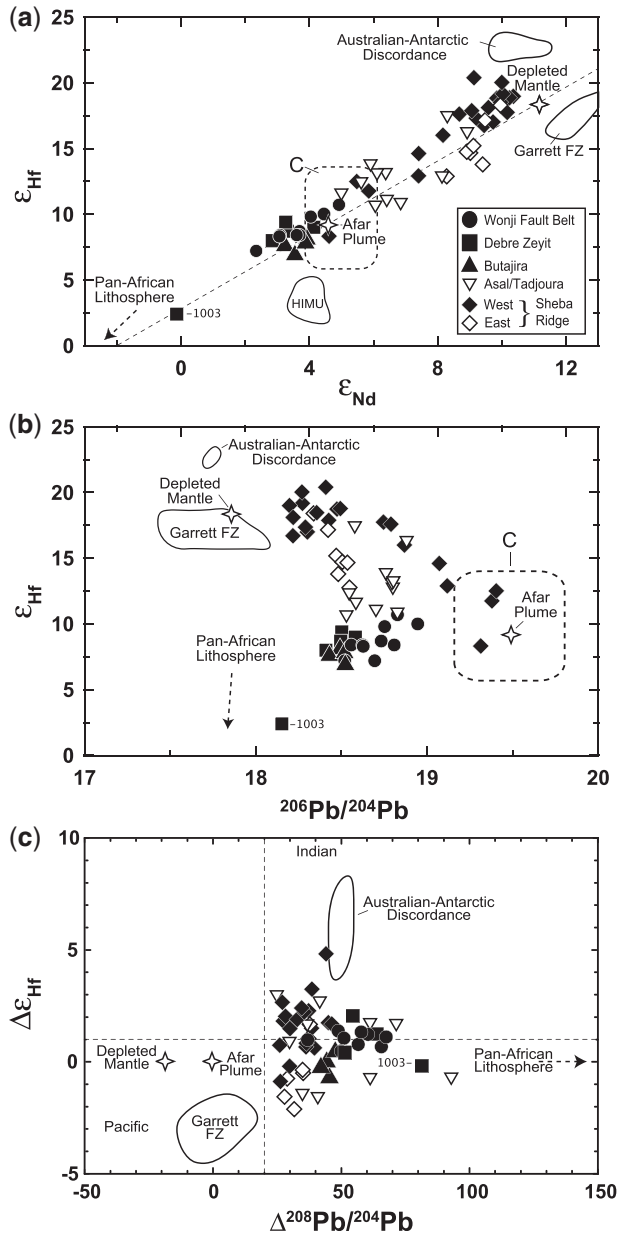### Afar plume–continental lithosphere–depleted mantle mixing model

The Arabian–Nubian shield represents Precambrian microplate accretion of inter-continental arcs, slivers of back-arc oceanic lithosphere, and older Precambrian terranes reactivated during Pan-African thermotectonic events (Schilling *et al.*, 1992; Be'eri-Shlevin *et al.*, 2010). The Pan-African sub-continental lithosphere is of variable mean age, origin, and isotopic composition; there are very

Table 5: F-test analysis of the similarities of the WFB, Butajira and Debre Zeyit in Pb isotope space

Pb isotopes	Region	Test	F-value	Degrees of freedom	F-crit. (95% confidence)	Is the group different from pooled?
206–208	WFB	Slope	0·58	27	4·2	No
		Elevation	19·33	28	4·2	Yes
	DZ	Slope	5·94	27	4·2	Yes
		Elevation	2·43	28	4·2	No
	BJ	Slope	0·37	27	4·2	No
		Elevation	60·2	28	4·2	Yes
207–206	WFB	Slope	0·01	27	4·2	No
		Elevation	9·79	28	4·2	Yes
	DZ	Slope	15·68	27	4·2	Yes
		Elevation	5·44	28	4·2	Yes
	BJ	Slope	2·9	27	4·2	No
		Elevation	67·48	28	4·2	Yes

The primary question posed was whether each of the three recognized geographical groups (BJ, Butajira; DZ, Debre Zeyit; WFB, Wonji Fault Belt) were distinctive on the basis of their isotopic results. As discussed in the text, Pb isotopes form distinctive linear arrays and hence can be used to examine differences and similarities between the groups. To establish whether each of the groups is distinctive from the dataset as a whole, we examined the slope and elevation of the arrays generated by $^{206}Pb/^{204}Pb–^{208}Pb/^{204}Pb$ and $^{206}Pb/^{204}Pb–^{207}Pb/^{204}Pb$. The F-test specifically asked: Are the Wonji Fault Belt, Debre Zeyit and Butajira samples distinctive from the remaining dataset in terms of slope and elevation? F-values were calculated using established methods (Snedecor & Cochran, 1989). F-crit. is the critical F-value (Davis, 1973) based on the degrees of freedom of the dataset; where the F-value is above the F-crit. value, the null hypothesis (that the slope and/or intercept of the respective datasets are identical) can be rejected at the 95% confidence level.

few published xenolith isotope data from the Arabian–Nubian shield. Radiogenic isotope analyses of mantle xenoliths from beneath Arabia (Yemen and Kod Ali Island in the Red Sea; Baker *et al.*, 2002) indicate that the lithosphere has been extensively modified by interaction with the plume and the asthenosphere, and in fact could be modelled by these same three end-members. The rejuvenated Pan-African lithosphere is not conducive to preserving ancient high $^{3}He/^{4}He$. Lithosphere with high time-integrated $^{3}He/(U + Th)$ that would allow preservation of ancient ^{3}He enrichments cannot exist within or below the continents, and is unlikely to exist within the upper mantle, based on $^{3}He/^{4}He$ in MORB (Day *et al.*, 2005).

The source origin of the Main Ethiopian Rift basalts cannot be solely within the sub-continental lithosphere. In the $^{208}Pb/^{204}Pb$ and $^{207}Pb/^{204}Pb$ vs $^{206}Pb/^{204}Pb$ isotope diagrams the new combined data do not fall along a single linear correlation, ruling out a simple binary source mixing origin for the lavas. At least three end-member components are required to account for the entire dataset. The three-component mixing model invoked by Schilling *et al.* (1992) for the mantle source of the lavas from the Gulf of Aden, its extension into the Gulf of Tadjoura, and subaerial basalts from the Ardoukoba Rift in east Afar calls upon interaction between a mantle plume, EM-like Pan-African continental lithosphere and the MORB-source asthenosphere, to explain the Nd–Sr–Pb isotope compositions. In general, these three end-members enclose the entire range of the Nd–Sr–Pb isotope ratios of the new Main Ethiopian Rift data presented here. Schilling *et al.* (1992) associated the Afar plume with a HIMU radiogenic Pb isotope signature. However, the Butajira, Debre Zeyit, and Wonji Fault Belt trends converge at a lower $^{206}Pb/^{204}Pb$ (∼19·6) than the characteristic HIMU value ($^{206}Pb/^{204}Pb$ >20; Zindler & Hart, 1986), consistent with an Afar plume composition similar to 'C' (Fig. 4), the 'common' isotopic composition observed in oceanic basalts (Hanan & Graham, 1996). This observation is further supported by the ε_{Nd} vs ε_{Hf} diagram, in which the Wonji Fault Belt, Debre Zeyit, and Butajira data trends all fall above and parallel to the mantle array, and do not show mixing relationships toward the HIMU composition, which plots below the mantle array (Fig. 5). In terms of three-component mixing, in addition to the relatively high $^{206}Pb/^{204}Pb$ plume end-member, the Main Ethiopian Rift data distribution requires the other two end-members to have lower $^{206}Pb/^{204}Pb$, with one having relatively higher $^{207}Pb/^{204}Pb$ than the other. These constraints are consistent with the Pan-African continental lithosphere (high $^{207}Pb/^{204}Pb$) and the asthenosphere (MORB-source mantle with low $^{207}Pb/^{204}Pb$) end-members of the Schilling *et al.* (1992) model for the Gulf of Aden, Gulf of Tadjoura, and Afar basalts. Here we retain the isotopic composition of the Pan-African lithosphere and depleted mantle end-members proposed by Schilling *et al.* (1992). We further extend and modify the three-component

Fig. 5. (a) ε_{Hf} vs ε_{Nd} and (b) $^{206}Pb/^{204}Pb$ vs ε_{Hf} for the Quaternary Main Ethiopian Rift sample suite and for the Gulf of Aden basalts [Nd and Pb isotopic data from Schilling *et al.* (1992)]. Model end-members (see Table 6) are shown as black open stars for the Afar plume and depleted mantle. Pan-African lithosphere plots off the diagram at this scale. The dashed-line field represents the range of values for C (Hanan & Graham, 1996; Hanan *et al.*, 2000). The fields for HIMU, depleted Indian Ocean MORB from the Australian–Antarctic Discordance region of the Southeast Indian Ridge, and depleted Pacific MORB from the East Pacific Rise Garrett Fracture Zone are also shown for reference (data from Chaffey *et al.*, 1989; Salters & White, 1998; Wendt *et al.*, 1999; Hanan *et al.*, 2004). The mantle array in (a) (dashed line) is represented by $\varepsilon_{Hf} = 1\cdot4\varepsilon_{Nd} + 2\cdot8$ (J. Blichert-Toft, unpublished compilation of >3000 oceanic basalts). Symbols are the same as in previous plots. (c) $\Delta^{208}Pb/^{204}Pb$ vs $\Delta\varepsilon_{Hf}$ for the most depleted MORB from the Pacific and Indian Ocean basins, represented by the Garrett Fracture Zone (Wendt *et al.*, 1999) and the Australian–Antarctic Discordance on the

Southeast Indian Ridge (after Hanan *et al.*, 2004). Pacific MORB have $\Delta^{208}Pb/^{204}Pb < 20$, whereas Indian Ocean MORB have $\Delta^{208}Pb/^{204}Pb > 20$. In terms of $\Delta\varepsilon_{Hf}$, the Pacific data are confined to the SW quadrant of the diagram with $\Delta\varepsilon_{Hf} < 1$. Depleted Indian Ocean MORB have positive $\Delta\varepsilon_{Hf}$, and plot in the NE quadrant with $\Delta\varepsilon_{Hf} > 1$. The distinction between the Pacific and Indian Ocean MORB derives from pollution of the mantle source of the latter by continental material (Hanan *et al.*, 2004). The data for the Main Ethiopian Rift and the Gulf of Aden show Hf and Pb isotope signatures similar to those of Indian Ocean MORB derived from mantle sources polluted with continental material. Debre Zeyit sample DZ-1003 is labeled.

Table 6: Isotope composition and elemental abundances for the model end-members

	Sr (ppm)	Nd (ppm)	Pb (ppm)	$^{87}Sr/^{86}Sr$	$^{143}Nd/^{144}Nd$	$^{206}Pb/^{204}Pb$	$^{207}Pb/^{204}Pb$	$^{208}Pb/^{204}Pb$
Afar plume	160	14	29	0·7035	0·512875	19·5	15·6	39·2
DM	75	4	5	0·7022	0·51335	17·5	15·3	36·6
Pan-African	225	22	39	0·7075	0·5121	17·85	15·75	39·75

These values are identical to those reported by Schilling *et al.* (1992) with the exception of the Afar plume end-member. Based on the present study, the Afar plume is now considered to be of a C mantle composition (Hanan & Graham, 1996) and the average isotopic values of C are used here. DM, depleted mantle; Pan African, Pan-African lithosphere. [See the Appendix of this paper and Schilling *et al.* (1992, appendix) for more model details.]

mixing model between the Afar plume, depleted upper mantle, and Pan-African lithosphere proposed by Schilling *et al.* (1992) and apply the model to the new Main Ethiopian Rift data (Tables 1–6).

In summary, the three end-member isotope compositions for the Main Ethiopian Rift ternary mixing model are dictated by the following constraints (see also Schilling *et al.*, 1992 for additional detail): (1) they must span the entire Main Ethiopian Rift dataset in Pb–Nd–Hf–Sr multi-isotope space (i.e. define a triangular space that surrounds the Main Ethiopian Rift dataset); (2) the convergence of the three pseudo-binary mixing trends for the Debre Zeyit, Butajira, and Wonji Fault Belt sub-populations constrains the composition of the radiogenic Pb end-member (the Afar plume); (3) the Afar plume has the isotopic composition of C (Hanan & Graham, 1996; Hanan *et al.*, 2000); (4) the least radiogenic of the two low $^{206}Pb/^{204}Pb$ end-members is assumed to represent the depleted asthenosphere sampled along normal mid-ocean ridge segments; (5) the low $^{206}Pb/^{204}Pb$ with a relatively high $^{207}Pb/^{204}Pb$ lithospheric-like end-member represents Pan-African lithosphere and is EM-like in its isotopic composition. We retain the Nd, Sr, and Pb isotopic compositions and elemental concentrations of the Pan-African lithosphere and depleted asthenosphere components used by Schilling *et al.* (1992). The Main Ethiopian Rift mixing model differs from the previous model in the choice of the Afar plume isotope composition, as outlined above. The Hf isotope data (Tables 1 and 2; Figs 4 and 5a) for the Gulf of Aden and the Main Ethiopian Rift strongly support the suggestion that the Afar plume composition is C-like rather than of HIMU composition.

The choice of end-members and the validity of the three-component mixing model deduced from the Pb isotope data were tested using principal component analysis (Fig. 6; for an explanation of principal component analysis applied to basalts see, for example, Schilling *et al.*, 1992;
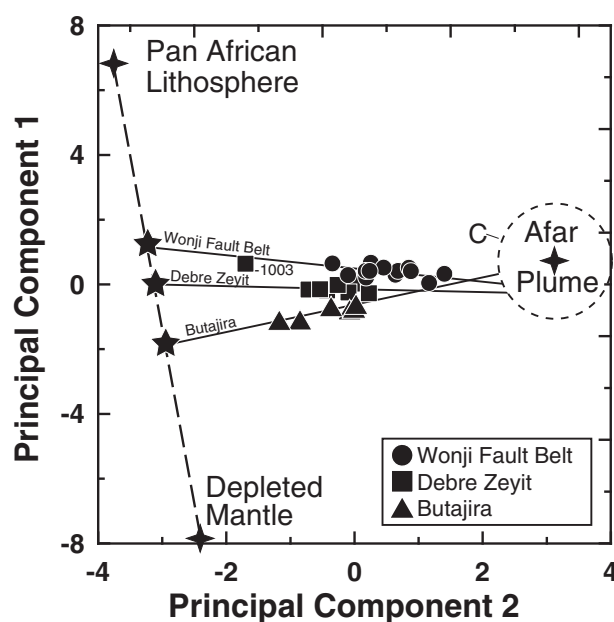

Fig. 6. PC1–PC2 projection of a principal component analysis for $^{206}Pb/^{204}Pb$, $^{207}Pb/^{204}Pb$, $^{208}Pb/^{204}Pb$, ε_{Nd}, and ε_{Sr} using the Main Ethiopian Rift data and the end-members defined in Table 6. The lines are least-squares regressions through the three sub-populations of data from Debre Zeyit, Butajira, and the Wonji Fault Belt. The labeled point (DZ-1003) was included in the principal component analysis, but omitted from the Debre Zeyit regression because it contains norite xenoliths and may have been affected by crustal assimilation associated with volcanism at a nearby silicic volcanic center (Rooney *et al.*, 2005). The eigenvectors PC1 =70·9% and PC2 =27·2% account for >98·1% of the total variance. The three-component mixing model is justified because two principal components (and thus, three geochemical end-members) sufficiently account for the Sr–Nd–Pb isotopic variability in the Main Ethiopian Rift lavas, and the three end-members lie within a single plane of mixing. The approximate field of the C-like Afar plume is shown as a dashed-line circle.

Hanan & Schilling, 1997; Blichert-Toft *et al.*, 2003, 2005; Agranier *et al.*, 2005; Debaille *et al.*, 2006). Considering only the Pb isotopes, 99·5% of the population variance is accounted for within the plane of the first two

eigenvectors. Principal component analysis using ^{206}Pb/^{204}Pb–^{207}Pb/^{204}Pb–^{208}Pb/^{204}Pb–^{87}Sr/^{86}Sr–^{143}Nd/^{144}Nd yields an equivalent result, with the first two eigenvectors accounting for 98·1% of the variance. Hf isotopes were not included given the smaller dataset and the principal component analysis requirement that each sample has the same number of variables. Furthermore, we have not assigned Hf isotope values to the end-members because (1) there are few or no Hf isotope data available to characterize the continental lithosphere in this region, and (2) the sparse Hf isotope data for the Main Ethiopian Rift and East African Rift in general do not currently show enough spread to determine accurate mixing trajectories. The principal component analysis results suggest that hyperbolic mixing of the geochemical end-members is minimal; that is, the elemental ratios of Pb, Sr, and Nd, in the hybrid end-member (comprising asthenospheric upper mantle and a small proportion of continental lithosphere) are approximately equal to those in the Afar plume end-member, resulting in linear mixing trends in multi-isotope ratio plots (e.g. Hanan & Schilling, 1997; Douglass & Schilling, 2000). The linear arrays in multi-isotope space define converging pseudo-binary mixing trends (Figs 3, 4 and 6). The converging trends for the Wonji Fault Belt, Debre Zeyit, and Butajira lavas apparently result from a special case of ternary mixing (case 3 described by Douglass & Schilling, 2000) in which the mass proportions of two of the end-members (depleted upper mantle and continental lithosphere) co-vary systematically along the rift, maintaining an essentially fixed ratio within each extensional zone. This type of mixing (in which the ratio of asthenosphere to continental lithosphere mass fraction is nearly constant, whereas the ratio of plume to asthenosphere markedly varies) is difficult to attribute to a single-stage mixing event, because in that case all of the components should be equally well mixed (Douglass & Schilling, 2000). An ordered, two-stage mixing process is required, during which the asthenosphere and continental lithosphere interact to form a hybrid, before mixing with the Afar plume.

We carried out the three-component Pb, Sr, and Nd isotope mixing model using basic principles described previously (Schilling *et al.*, 1992; Hanan & Schilling, 1997; Douglass & Schilling, 2000; Hanan *et al.*, 2000) (Fig. 7). The modeling indicates that the mixtures are dominated by the asthenosphere (depleted mantle component) (mass fraction = 49–80%), and that the mass fraction of the Afar plume (C-like Afar plume component) (10–43%) is larger than that of the continental lithosphere (Pan-African lithosphere component) (6–17%). The mass fractions of the plume and depleted mantle components co-vary ($r^2 = 0.92$), and the contribution from the Afar plume decreases systematically away from the hypothesized plume center beneath Lake Abhe (Schilling *et al.*, 1992)

(Fig. 7). The ^{3}He/^{4}He ratio (Table 3) broadly co-varies positively with the mass proportion of the Afar plume in the three-component mixture, providing further evidence that the converging pseudo-binary mixing arrays in isotope–isotope space can be used to constrain the Pb–Sr–Nd isotopic composition of the Afar plume component.

Quaternary basalts (MgO >7 wt %) from the Djibouti and Red Sea region [e.g. the Quaternary Moussa Ali volcano and the Maranda-Inkir volcanic centers located NE of the Afar plume center, and from the Sept Frères volcanic islands in the Red Sea (Deniel *et al.*, 1994)] provide additional support for the model of radial dispersion from a plume centered beneath the Lake Abhe region (Fig. 4). The Djibouti and Red Sea data fall along extensions of the converging Pb isotope trends for the Main Ethiopian Rift lavas, within the region defined by the three-component mixing model end-members.

Plume–lithosphere interaction in the East African Rift system

Previous studies have shown that the extent of upper mantle pollution in the vicinity of an upwelling and dispersing plume decreases systematically with radial distance from the plume center (Schilling, 1985; Hanan *et al.*, 1986; Hanan & Schilling, 1989). Afar plume influence has been observed to extend from Afar for ∼700 km along the Gulf of Aden, into the Red Sea, and along the Ethiopian sector of the East African Rift (Barrat *et al.*, 1990; Schilling *et al.*, 1992; Marty *et al.*, 1993, 1996; Deniel *et al.*, 1994; Scarsi & Craig, 1996; Moreira *et al.*, 1999; Hopp *et al.*, 2004). The Afar plume head is envisioned to have flattened beneath the lithosphere like a pancake, and now has a radial influence of the order of 700–1400 km (Schilling *et al.*, 1992; Volker *et al.*, 1997).

Based on the laboratory models of Griffiths & Campbell (1990), Schilling *et al.* (1992) proposed that the flattened Afar plume head has a torus-like structure, containing an outer ring of deeply derived material located about 450 km (± 150 km) from the center of the upwelling, and an inner region of entrained, depleted mantle. In this model the plume tail appears to be tilted toward Afar (Schilling *et al.*, 1992). Along the Sheba Ridge an anomaly in radiogenic Pb, Sr, Nd, and Hf isotopes is located above the proposed torus ring. East of the anomaly (48°E) the MORB are LILE-depleted and show a slight increase in radiogenic Pb and Sr isotope compositions (Schilling *et al.*, 1992). To the west of the anomaly, lavas from the Gulf of Tadjoura and Asal Rift are more similar to the Main Ethiopian Rift lavas compared with the West Sheba Ridge MORB, and have Pb, Sr, Nd, and Hf isotope compositions that indicate a greater involvement of continental lithosphere in their genesis. The western part of the proposed torus would underlie the Main Ethiopian Rift in
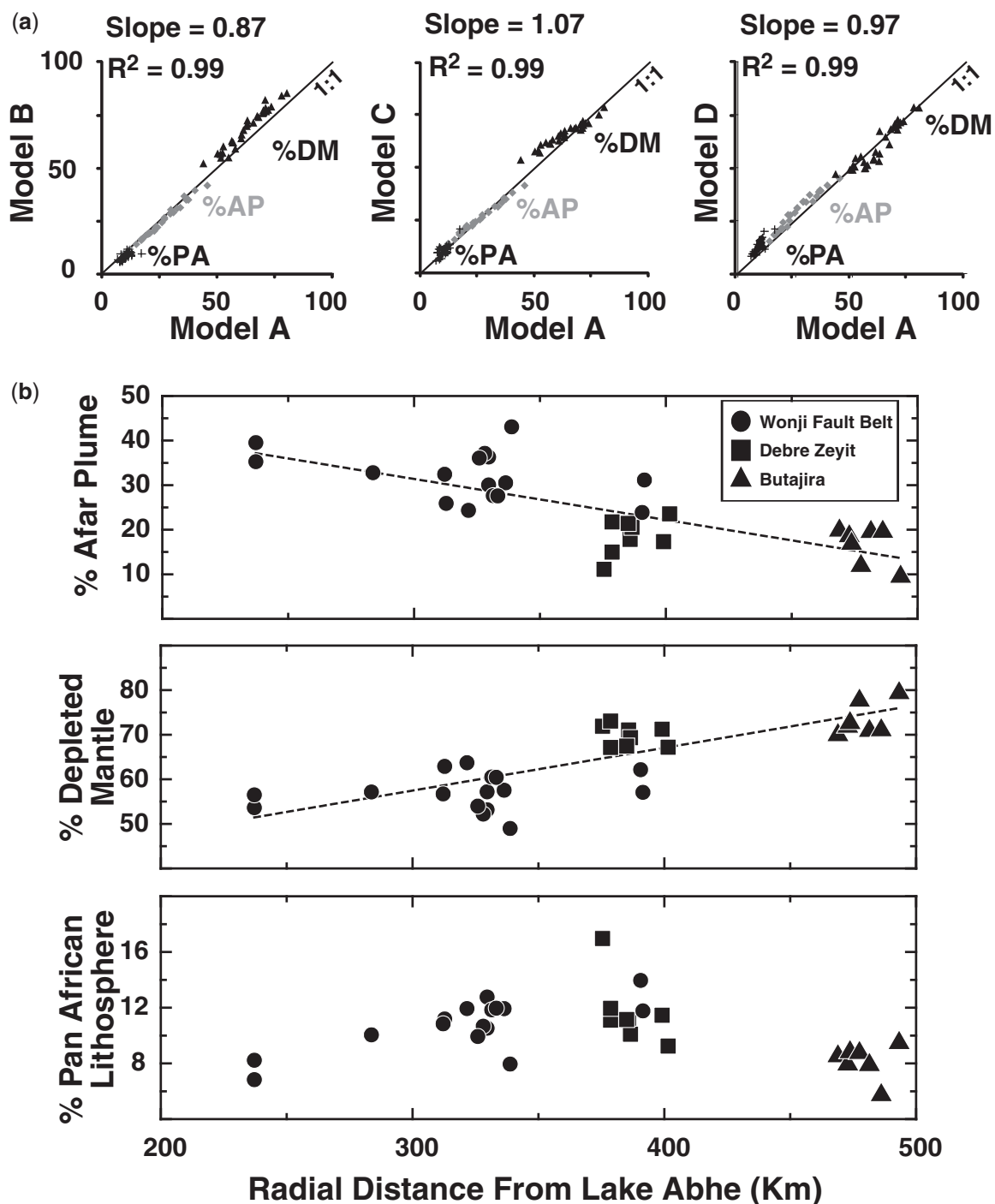
Fig. 7. (a) Correlation diagrams for mixing model solutions. With this model, a complete solution providing the percentage of plume, depleted mantle, and continental lithosphere for a single sample can only be determined using two isotope ratios at a time. Thus each 'model' uses a pair of isotopes from each sample to yield percentages of each component (PA, Pan-African; AP, Afar plume; DM, depleted mantle). We have compared the results of using one pair of isotopes with an alternate pair to test the model's self-consistency. Model A $= ^{207}Pb/^{204}Pb-^{206}Pb/^{204}Pb$, Model B $= ^{208}Pb/^{204}Pb-^{206}Pb/^{204}Pb$, Model C $= ^{143}Nd/^{144}Nd-^{206}Pb/^{204}Pb$, Model D $= ^{87}Sr/^{86}Sr-^{206}Pb/^{204}Pb$. The model (A–D) end-member proportions for each Main Ethiopian Rift sample from Table 1 are presented in Appendix Table A2. The slopes vary from 0·87 to 1·07 and r^2 is consistently 0·99, indicating that the mixing model is robust and adequately accounts for the isotope variability of the Main Ethiopian Rift samples (Wonji Fault Belt, Debre Zeyit, Butajira). Details of the three-component mixing model are provided in the Appendix. For any sample, the percentage values of the three end-members that are given in the main text are an average of the values derived from the four models (A–D) presented above. (b) Spatial variation of the mass proportions of Afar plume, depleted mantle and Pan-African lithospheric components deduced from our modeling along the East African Rift. The distance in kilometers (Table 1) represents the great circle radial distance from the plume center in the Lake Abhe region (Schilling *et al.*, 1992). There is a systematic decrease in plume mass proportion and increase in depleted mantle proportion away from the plume center.

southernmost Ethiopia, where the plume tail is supposedly tilted toward the west. Geophysical studies have not imaged a distinct tail structure, but instead show a broad low-velocity structure tilted westward (Benoit *et al.*, 2006). According to the torus model, our new Main Ethiopian Rift sample locations would correspond to a traverse from inside the plume torus towards and across the edge of the proposed location of the western ring. The observed gradient of decreasing radiogenic Pb, Sr, and Nd away from the plume center and toward the proposed ring location is opposite to what would be predicted by the torus model. Furthermore, melting in the center of the torus plume was suggested to be dominated by lithospheric mantle and depleted asthenosphere entrained by the plume. However, based on the regular spatial variations in the Pb–Sr–Nd–Hf–He isotope ratios along the Main Ethiopian Rift, and the results of our mixing model, it is apparent that all three mantle source components, Pan-African lithosphere, depleted mantle, and the Afar plume, contribute to the petrogenesis of the Main Ethiopian Rift basalts located in the region of the proposed inner ring. The Asal rift and the Gulf of Tadjoura lavas have Pb isotope ratios consistent with radial dispersion of the plume and their distance of about 150–300 km from the plume center. We observe a gradient in plume influence (Figs 2 and 7) along the Main Ethiopian Rift that is expressed by a systematic co-variation between plume and depleted asthenosphere mass fractions (Fig. 7). The near-constant ratio of African continental lithosphere to depleted upper mantle for each of the extensional zones, revealed by the pseudo-binary arrays for the Wonji Fault Belt, Debre Zeyit, and Butajira subgroups, requires two stages of mixing (Douglass & Schilling, 2000). The first stage involves mixing of asthenospheric mantle and continental lithosphere, followed by a second stage during which this hybrid upper mantle mixes with the Afar plume. Detachment and foundering of lithosphere during rifting is one mechanism for contaminating the upper mantle with continental material (Arndt & Goldstein, 1989). This process may occur when the lithosphere becomes ductile, as a result of thermal or flexural weakening during extension (Burov *et al.*, 2007). The hot Afar plume head beneath the rift also contributes to thermal weakening by conductive heating. As the lithosphere is heated and thinned during plume impingement and incipient rifting (e.g. Kent *et al.*, 1992), portions of the uppermost mantle beneath the lithospheric mechanical boundary layer (McKenzie & Bickle, 1988) are admixed with lithospheric material. This upper mantle pollution with continental lithospheric material occurs prior to when the uppermost mantle becomes a sink for the buoyant and dispersing plume (Sleep, 2008). This process is influenced by the underside topography of the continental lithosphere, which may channel plume material into 'thin spots' without involving plume-driven thinning

(Thompson & Gibson, 1991; Ebinger & Sleep, 1988; Sleep *et al.*, 2002; Shervais & Hanan, 2008). For example, the isotopic anomaly on the West Sheba Ridge adjacent to the transition between continental and oceanic lithosphere may relate to a step decrease in lithospheric thickness that acts as a sink for plume material (Fig. 2c). The two-stage ordered mixing along the Main Ethiopian Rift suggests that the sub-continental lithosphere acted as a levee against plume flow along the rift until the tectonic forces and geometry of extension associated with the triple junction creation led to formation of the Main Ethiopian Rift arm.

Implications for the composition of the upper mantle

The sequence of mixing described above has implications for the origin of upper mantle heterogeneity, as well as for the composition and origin of mantle plumes. Asthenospheric mantle that was once associated with continental rifting may retain evidence of continental lithosphere contamination (McKenzie & O'Nions, 1983; Hawkesworth *et al.*, 1986; Arndt & Goldstein, 1989; Hanan & Graham, 1996; Hanan *et al.*, 2004). Pollution of the upper mantle by continental lithosphere (and/or lower crust) has been observed in the Tertiary basalts of Iceland (Hanan & Schilling, 1997; Hanan *et al.*, 2000), along the Mid-Atlantic Ridge north of Iceland (Andres *et al.*, 2004; Blichert-Toft *et al.*, 2005) and along the Gakkel Ridge in the Arctic (Goldstein *et al.*, 2008), in the South Atlantic (Hawkesworth *et al.*, 1986; Carlson *et al.*, 1996; Kamenetsky *et al.*, 2001; Andres *et al.*, 2002) and along the Southwest (Escrig *et al.*, 2005; Janney *et al.*, 2005; Meyzen *et al.*, 2007) and Southeast Indian Ridges (Hanan *et al.*, 2004; Graham *et al.*, 2006). Our observations and model for the Ethiopian sector of the East African Rift indicate that mantle plume material interacts with continental lithosphere and upper mantle only after thermomechanical thinning of the lithosphere has progressed sufficiently to form a sink for the rising and dispersing plume material. Lithospheric detachment and mixing into the asthenosphere during continental rift evolution may, therefore, account for much of the range of ambient upper mantle compositions sampled by mid-ocean ridge volcanism away from island hotspots. A corollary is that the isotopic composition of plume-related lavas, such as continental flood basalts and some oceanic islands, may not always represent the isotopic composition of the deep mantle plume source alone, but instead carry an integrated record of plume interaction and mixing with upper mantle that has been variably polluted with continental material such as the Yellowstone Plume (Hanan *et al.*, 2008) and eastern Atlantic cases (Geldmacher *et al.*, 2011).

CONCLUSIONS

The isotopic variations of basalts erupted along the Main Ethiopian Rift at Debre Zeyit, Butajira, and the Wonji Fault Belt result from mixing between the Afar plume, the asthenospheric upper mantle and the African continental lithosphere. The isotopic composition of the Afar plume resembles the 'C' component on the basis of converging arrays in multi-isotope space. The influence of this plume signature systematically decreases along the Main Ethiopian Rift away from Afar into southern Ethiopia. Mixing between the plume, lithosphere, and ambient upper mantle follows an ordered sequence of events. Within each volcanic belt the Afar plume mixes with a hybrid reservoir that is composed of different proportions of lithosphere and depleted mantle. Within each volcanic belt, the mass proportions of continental lithosphere and upper mantle are relatively constant, requiring that the mixing event that generated these hybrid reservoirs occurred prior to their mixing with the Afar plume.

Detachment and dispersal of continental lithosphere into the upper mantle during plume–rift interaction follows an ordered sequence of mixing events. This mixing produces large-scale pollution of the upper mantle by continental lithosphere that is recorded in the 'background' geochemical signatures of MORB, even those erupting far away from mantle hotspots or plumes. Furthermore, the distinct isotopic compositions of plume-related lavas may not necessarily represent intrinsic mantle source signatures, but rather a complex history of mixing involving components derived from both the upper and lower mantle.

SUPPLEMENTARY DATA

Supplementary data for this paper are available at *Journal of Petrology* online.

REFERENCES

Agranier, A., Blichert-Toft, J., Graham, D., Debaille, V., Schiano, P. & Albarède, F. (2005). The spectra of isotopic heterogeneities along the mid-Atlantic Ridge. *Earth and Planetary Science Letters* **238(1–2)**, 96–109.

Albarède, F. (1995). *Introduction to Geochemical Modelling*. Cambridge: Cambridge University Press, 543 p.

Altherr, R., Henjes-Kunst, F., Puchelt, H. & Baumann, A. (1988). Volcanic activity in the Red Sea axial trough—evidence for a large mantle diapir. *Tectonophysics* **150(1–2)**, 121–133.

Andres, M., Blichert-Toft, J. & Schilling, J. G. (2002). Hafnium isotopes in basalts from the southern Mid-Atlantic Ridge from 40°S to 55°S: Discovery and Shona plume–ridge interactions and the role of recycled sediments. *Geochemistry, Geophysics, Geosystems* **3**, 8502, doi:10.1029/2002gc000324.

Andres, M., Blichert-Toft, J. & Schilling, J. G. (2004). Nature of the depleted upper mantle beneath the Atlantic: evidence from Hf isotopes in normal mid-ocean ridge basalts from 79°N to 55°S. *Earth and Planetary Science Letters* **225(1–2)**, 89–103.

Arndt, N. T. & Goldstein, S. L. (1989). An open boundary between lower continental-crust and mantle—Its role in crust formation and crustal recycling. *Tectonophysics* **161(3–4)**, 201–212.

Baker, J., Chazot, G., Menzies, M. A. & Thirlwall, M. (2002). Lithospheric mantle beneath Arabia: A Pan-African protolith modified by the Afar and older plumes, rather than a source for continental flood volcanism. In: Menzies, M. A., Klemper, S. L., Ebinger, C. & Baker, J. (eds) *Volcanic Rifted Margins*. Geological Society of America: Special Papers **362**, 65–80.

Barrat, J. A., Jahn, B. M., Joron, J. L., Auvray, B. & Hamdi, H. (1990). Mantle heterogeneity in Northeastern Africa—Evidence from Nd isotopic compositions and hygromagmaphile element geochemistry of basaltic rocks from the Gulf of Tadjoura and Southern Red Sea Regions. *Earth and Planetary Science Letters* **101(2–4)**, 233–247.

Barrat, J. A., Fourcade, S., Jahn, B. M., Cheminee, J. L. & Capdevila, R. (1998). Isotope (Sr, Nd, Pb, O) and trace-element geochemistry of volcanics from the Erta'Ale range (Ethiopia). *Journal of Volcanology and Geothermal Research* **80(1–2)**, 85–100.

Be'eri-Shlevin, Y., Katzir, Y., Blichert-Toft, J., Kleinhanns, I. C. & Whitehouse, M. J. (2010). Nd–Sr–Hf–O isotope provinciality in the northernmost Arabian–Nubian Shield: implications for crustal evolution. *Contributions to Mineralogy and Petrology* **160(2)**, 181–201.

Benoit, M. H., Nyblade, A. A. & VanDecar, J. C. (2006). Upper mantle P-wave speed variations beneath Ethiopia and the origin of the Afar hotspot. *Geology* **34(5)**, 329–332.

Blichert-Toft, J., Chauvel, C. & Albarède, F. (1997). Separation of Hf and Lu for high-precision isotope analysis of rock samples by magnetic sector multiple collector ICP-MS. *Contributions to Mineralogy and Petrology* **127(3)**, 248–260.

Blichert-Toft, J., Weis, D., Maerschalk, C., Agranier, A. & Albarède, F. (2003). Hawaiian hot spot dynamics as inferred from the Hf and Pb isotope evolution of Mauna Kea volcano. *Geochemistry, Geophysics, Geosystems* **4**, 8704, doi:10.1029/2002GC000340.

Blichert-Toft, J. & Albarède, F. (1997). The Lu-Hf isotope geochemistry of chondrites and the evolution of the mantle-crust system. *Earth and Planetary Science Letters* **148**, 243–258.

Blichert-Toft, J., Agranier, A., Andres, M., Kingsley, R., Schilling, J. G. & Albarède, F. (2005). Geochemical segmentation of the Mid-Atlantic Ridge north of Iceland and ridge–hot spot interaction in the North Atlantic. *Geochemistry, Geophysics, Geosystems* **6**, Q01E19, doi:10.1029/2004GC000788.

Burke, K. & Wilson, J. T. (1972). Is the African Plate stationary? *Nature* **239**, 387–390.

Burov, E., Guillou-Frottier, L., d'Acremont, E., Le Pourhiet, L. & Cloetingh, S. (2007). Plume head–lithosphere interactions near intra-continental plate boundaries. *Tectonophysics* **434(1–4)**, 15–38.

Camp, V. E. & Hanan, B. B. (2008). A plume-triggered delamination origin for the Columbia River Basalt Group. *Geosphere* **4**, 480–495.

Camp, V. E. & Ross, M. E. (2004). Mantle dynamics and genesis of mafic magmatism in the intermontane Pacific Northwest. *Journal of Geophysical Research* **109(B08204)**, 14, doi:10.1029/2003JB002838.

Campbell, I. H. & Griffiths, R. W. (1990). Implication of mantle plume structure for the evolution of flood basalts. *Earth and Planetary Science Letters* **99**, 79–93.

Carlson, R. W., Esperanca, S. & Svisero, D. P. (1996). Chemical and Os isotopic study of Cretaceous potassic rocks from southern Brazil. *Contributions to Mineralogy and Petrology* **125(4)**, 393–405.

Carlson, R. W., Pearson, D. G. & James, D. E. (2005). Physical, chemical, and chronological characteristics of continental mantle. *Reviews of Geophysics* **43(1)**, RG1001, doi:10.1029/2004RG000156.

Casey, M., Ebinger, C., Keir, D., Gloaguen, R. & Mohamed, F. (2006). Strain accomadation in transitional rifts: Extension by magma intrusion and faulting in Ethiopian rift magmatic segments. In: Yirgu, G., Ebinger, C. & Maguire, P. (eds) *The Afar Volcanic Province within the East African Rift System*. Geological Society, London: Special Publications **259**, 143–164.

Chaffey, D. J., Cliff, R. A. & Wilson, B. M. (1989). Characterization of the St Helena magma source. In: Saunders, A. D. & Norry, M. J. (eds) *Magmatism in the Ocean Basins*. Geological Society, London: Special Publications **42**, 257–276.

Class, C. & le Roex, A. P. (2006). Continental material in the shallow oceanic mantle—How does it get there? *Geology* **34(3)**, 129–132.

Courtney, R. & White, R. (1986). Anomalous heat flow and geoid across the Cape Verde Rise: evidence for dynamic support from a thermal plume in the mantle. *Geophysical Journal of the Royal Astronomical Society* **87**, 815–867.

Crough, S. T. (1978). Thermal origin of mid-plate hotspot swells. *Geophysical Journal of the Royal Astronomical Society* **55**, 451–469.

Davis, J. C. (1973). *Statistical and Data Analysis in Geology*. New York: John Wiley, 550 p.

Day, J. M. D., Hilton, D. R., Pearson, D. G., Macpherson, C. G., Kjarsgaard, B. A. & Janney, P. E. (2005). Absence of a high time-integrated He-3/(U + Th) source in the mantle beneath continents. *Geology* **33(9)**, 733–736.

Debaille, V., Blichert-Toft, J., Agranier, A., Doucelance, R., Schiano, P. & Albarède, F. (2006). Geochemical component relationships in MORB from the Mid-Atlantic Ridge, 22–35°N. *Earth and Planetary Science Letters* **241(3–4)**, 844–862.

Deniel, C., Vidal, P., Coulon, C. & Vellutini, P. J. (1994). Temporal evolution of mantle sources during continental rifting—the volcanism of Djibouti (Afar). *Journal of Geophysical Research: Solid Earth* **99(B2)**, 2853–2869.

Detrick, R. S., Sinton, J. M., Ito, G., Canales, J. P., Behn, M., Blacic, T., Cushman, B., Dixon, J. E., Graham, D. W. & Mahoney, J. J. (2002). Correlated geophysical, geochemical, and volcanological manifestations of plume–ridge interaction along the Galápagos Spreading Center. *Geochemistry, Geophysics, Geosystems* **3**, 8501, doi:10.1029/2002GC000350.

Douglass, J. & Schilling, J. G. (2000). Systematics of three-component, pseudo-binary mixing lines in 2D isotope ratio space representations and implications for mantle plume–ridge interaction. *Chemical Geology* **163(1–4)**, 1–23.

Duncan, R. A. (1981). Hotspots in the Southern Oceans—an absolute frame of reference for motion of the Gondwana continents. *Tectonophysics* **74**, 29–42.

Ebinger, C. J. & Casey, M. (2001). Continental breakup in magmatic provinces: An Ethiopian example. *Geology* **29(6)**, 527–530.

Ebinger, C. J. & Sleep, N. H. (1988). Cenozoic magmatism throughout east Africa resulting from impact of a single plume. *Nature* **395**, 788–791.

Ebinger, C. J., Yemane, T., Harding, D. J., Tesfaye, S., Kelley, S. & Rex, D. C. (2000). Rift deflection, migration, and propagation: Linkage of the Ethiopian and Eastern rifts, Africa. *Geological Society of America Bulletin* **112(2)**, 163–176.

Ernst, R. E. & Buchan, K. L. (2003). Recognizing mantle plumes in the geologic record. *Annual Review of Earth and Planetary Sciences* **31**, 469–523.

Escrig, S., Schiano, P., Schilling, J. G. & Allegre, C. (2005). Rhenium–osmium isotope systematics in MORB from the Southern Mid-Atlantic Ridge (40°–50°S). *Earth and Planetary Science Letters* **235(3–4)**, 528–548.

Falcon, N. L., Gass, I. G., Girdler, R. W. & Laughton, A. S. (1970). A discussion on the structure and evolution of the Red Sea and the nature of the Red Sea, Gulf of Aden, and Ethiopia Rift Junction. *Philosophical Transactions of the Royal Society of London, Series A* **267**, 131–142.

Farnetani, C. G. & Richards, M. A. (1994). Numerical investigation of the mantle plume initiation model for flood basalt events. *Journal of Geophysical Research* **99**, 13813–13833.

Furman, T. (2007). Geochemistry of East African Rift basalts: an overview. *Journal of African Earth Sciences* **48(2–3)**, 147–160.

Furman, T., Bryce, J. G., Rooney, T., Hanan, B. B., Yirgu, G. & Ayalew, D. (2006). Heads and tails: 30 million years of the Afar plume. In: Yirgu, G., Ebinger, C. & Maguire, P. (eds) *The Afar Volcanic Province within the East African Rift System*. Geological Society, London: Special Publications **259**, 95–120.

Geldmacher, J., Hoernle, K., Hanan, B. B., Blichert-Toft, J., Hauff, F., Gill, J. B. & Schmincke, H.-U. (2011). Hafnium isotopic variations in East Atlantic intraplate volcanism. *Contributions to Mineralogy and Petrology* **162**, 21–36.

Girdler, R. W. (1970). A review of the Red Sea heat flow. *Philosophical Transactions of the Royal Society of London, Series A* **267**, 191–204.

Goldstein, S. L., Soffer, G., Langmuir, C. H., Lehnert, K. A., Graham, D. W. & Michael, P. J. (2008). Origin of a 'Southern Hemisphere' geochemical signature in the Arctic upper mantle. *Nature* **453(7191)**, 89–93.

Graham, D. W., Jenkins, W. J., Schilling, J. G., Thompson, G., Kurz, M. D. & Humphris, S. E. (1992). Helium isotope geochemistry of mid-ocean ridge basalts from the South Atlantic. *Earth and Planetary Science Letters* **110(1–4)**, 133–147.

Graham, D. W., Larsen, L. M., Hanan, B. B., Storey, M., Pedersen, A. K. & Lupton, J. E. (1998). Helium isotope composition of the early Iceland mantle plume inferred from the Tertiary picrites of West Greenland. *Earth and Planetary Science Letters* **160(3–4)**, 241–255.

Graham, D. W., Blichert-Toft, J., Russo, C. J., Rubin, K. H. & Albarède, F. (2006). Cryptic striations in the upper mantle revealed by hafnium isotopes in southeast Indian ridge basalts. *Nature* **440(7081)**, 199–202.

Graham, D. W., Reid, M. R., Jordan, B. T., Grunder, A. L., Leeman, W. P. & Lupton, J. E. (2009). Mantle source provinces beneath the Northwestern USA delimited by helium isotopes in

young basalts. *Journal of Volcanology and Geothermal Research* **188(1–3)**, 128–140.

Griffiths, R. W. & Campbell, I. H. (1990). Stirring and structure in mantle starting plumes. *Earth and Planetary Science Letters* **99(1–2)**, 66–78.

Griffiths, R. W. & Campbell, I. H. (1991). Interaction of mantle plume heads with the Earth's surface and onset small-scale convection. *Journal of Geophysical Research* **96**, 18275–18310.

Hanan, B. B. & Graham, D. W. (1996). Lead and helium isotope evidence from oceanic basalts for a common deep source of mantle plumes. *Science* **272(5264)**, 991–995.

Hanan, B. B. & Schilling, J. G. (1989). Easter microplate evolution—Pb isotope evidence. *Journal of Geophysical Research: Solid Earth and Planets* **94(B6)**, 7432–7448.

Hanan, B. B. & Schilling, J. G. (1997). The dynamic evolution of the Iceland mantle plume: the lead isotope perspective. *Earth and Planetary Science Letters* **151(1–2)**, 43–60.

Hanan, B. B., Kingsley, R. & Schilling, J. G. (1986). Pb isotope evidence in the South Atlantic for migrating ridge–hotspot interactions. *Nature* **322**, 137–144.

Hanan, B. B., Shervais, J. W. & Vetter, S. K. (2008). Yellowstone plume–continental lithosphere interaction beneath the Snake River Plain. *Geology* **36(1)**, 51–54.

Hanan, B. B., Blichert-Toft, J., Kingsley, R. & Schilling, J. G. (2000). Depleted Iceland mantle plume geochemical signature. *Geochemistry, Geophysics, Geosystems* **1**, 1003, doi:10.1029/1999GC000009.

Hanan, B. B., Blichert-Toft, J., Pyle, D. G. & Christie, D. M. (2004). Contrasting origins of the upper mantle revealed by hafnium and lead isotopes from the Southeast Indian Ridge. *Nature* **432(7013)**, 91–94.

Hart, S. R. (1984). A large-scale isotope anomaly in the southern-hemisphere mantle. *Nature* **309(5971)**, 753–757.

Hart, S. R., Hauri, E. H., Oschmann, L. A. & Whitehead, J. A. (1992). Mantle plumes and entrainment; isotopic evidence. *Science* **256(5056)**, 517–520.

Hart, W. K., Woldegabriel, G., Walter, R. C. & Mertzman, S. A. (1989). Basaltic volcanism in Ethiopia—Constraints on continental rifting and mantle interactions. *Journal of Geophysical Research: Solid Earth and Planets* **94(B6)**, 7731–7748.

Hauri, E. H., Whitehead, J. A. & Hart, S. R. (1994). Fluid dynamic and geochemical aspects of entrainment in mantle plumes. *Journal of Geophysical Research: Solid Earth* **99(B12)**, 24275–24300.

Hawkesworth, C. J., Mantovani, M. S. M., Taylor, P. N. & Palacz, Z. (1986). Evidence from the Parana of South Brazil for a continental contribution to Dupal basalts. *Nature* **322(6077)**, 356–359.

Hofmann, A. W. (1997). Mantle geochemistry: the message from oceanic volcanism. *Nature* **385**, 219–229.

Hofmann, A. W., Hemond, C., Sarbas, B. & Jochum, B. (2005). Yes, there really is a lead paradox. *EOS Transactions, American Geophysical Union* **86(52)** (Fall Meeting Supplement), Abstract V23D-05.

Hofmann, A. W., Jochum, K. P., Seufert, M. & White, W. M. (1986). Nb and Pb in oceanic basalts—New constraints on mantle evolution. *Earth and Planetary Science Letters* **79(1–2)**, 33–45.

Hofmann, C., Courtillot, V., Feraud, G., Rouchett, P., Yirgu, G., Ketefo, E. & Pik, R. (1997). Timing of the Ethiopian flood basalt event and implications for plume birth and global change. *Nature* **389(6653)**, 838–841.

Hopp, J., Trieloff, M. & Altherr, R. (2004). Neon isotopes in mantle rocks from the Red Sea region reveal large-scale plume–lithosphere interaction. *Earth and Planetary Science Letters* **219(1–2)**, 61–76.

Ingle, S., Weis, D., Scoates, J. S. & Frey, F. A. (2002). Relationship between the early Kerguelen plume and continental flood basalts of the paleo-Eastern Gondwanan margins. *Earth and Planetary Science Letters* **197**, 35–50.

Janney, P. E., Le Roex, A. P. & Carlson, R. W. (2005). Hafnium isotope and trace element constraints on the nature of mantle heterogeneity beneath the central Southwest Indian Ridge (13°E to 47°E). *Journal of Petrology* **46(12)**, 2427–2464.

Jones, S. M. & White, N. (2003). Shape and size of the starting Iceland plume swell. *Earth and Planetary Science Letters* **216**, 271–282.

Kamenetsky, V. S., Maas, R., Sushchevskaya, N. M., Norman, M. D., Cartwright, I. & Peyve, A. A. (2001). Remnants of Gondwanan continental lithosphere in oceanic upper mantle: Evidence from the South Atlantic Ridge. *Geology* **29(3)**, 243–246.

Kent, R. W., Storey, M. & Saunders, A. D. (1992). Large igneous provinces—Sites of plume impact or plume incubation. *Geology* **20(10)**, 891–894.

Leeman, W. P. & Hawkesworth, C. J. (1986). Open magma systems—trace-element and isotopic constraints. *Journal of Geophysical Research: Solid Earth and Planets* **91(B6)**, 5901–5912.

Lustrino, M. (2005). How the delamination and detachment of lower crust can influence basaltic magmatism. *Earth-Science Reviews* **72**, 21–38.

Mahoney, J., Le Roex, A. P., Peng, Z., Fisher, R. L. & Natland, J. H. (1992). Southwestern limits of Indian Ocean ridge mantle and the origin of low $^{206}Pb/^{204}Pb$ mid-ocean ridge basalt: isotope systematics of the central Southwest Indian Ridge (17°–50°E). *Journal of Geophysical Research* **97**, 19771–19790.

Mahoney, J. J., White, W. M., Upton, B. G. J., Neal, C. R. & Scrutton, R. A. (1996). Beyond EM-1: lavas from Afanasy-Nikitin Rise and the Crozet Archipelago, Indian Ocean. *Geology* **24**, 615–618.

Mahoney, J. J., Natland, J. H., White, W. M., Poreda, R., Bloomer, S. H., Fisher, R. L. & Baxter, A. N. (1989). Isotopic and geochemical provinces of the western Indian Ocean spreading centers. *Journal of Geophysical Research* **94**, 4033–4052.

Marty, B., Appora, I., Barrat, J.-A. A., Deniel, C., Vellutini, P., Vidal, P., Kusakabe, M. & Shinohara, H. (1993). He, Ar, Sr, Nd and Pb isotopes in volcanic rocks from Afar; evidence for a primitive mantle component and constraints on magmatic sources. *Geochemical Journal* **27(4–5)**, 219–228.

Marty, B., Pik, R. & Gezahegn, Y. (1996). Helium isotopic variations in Ethiopian plume lavas; nature of magmatic sources and limit on lower mantle contribution. *Earth and Planetary Science Letters* **144(1–2)**, 223–237.

McKenzie, D. & Bickle, M. J. (1988). The volume and composition of melt generated by extension of the lithosphere. *Journal of Petrology* **29(3)**, 625–679.

McKenzie, D. & O'Nions, R. K. (1983). Mantle reservoirs and ocean island basalts. *Nature* **301(5897)**, 229–231.

McKenzie, D. & O'Nions, R. K. (1995). The source regions of ocean island basalts. *Journal of Petrology* **36(1)**, 133–159.

McNutt, M. K. & Judge, A. V. (1990). The superswell and mantle dynamics beneath the South Pacific. *Science* **248**, 969–975.

Meyzen, C. M., Blichert-Toft, J., Ludden, J. N., Humler, E., Mevel, C. & Albarède, F. (2007). Isotopic portrayal of the Earth's upper mantle flow field. *Nature* **447(7148)**, 1069–1074.

Mohr, P. A. (1967). Major volcano-tectonic lineament in the Ethiopian rift system. *Nature* **213(5077)**, 664–665.

Moreira, M., Doucelance, R., Kurz, M. D., Dupre, B. & Allegre, C. J. (1999). Helium and lead isotope geochemistry of the Azores Archipelago. *Earth and Planetary Science Letters* **169(1–2)**, 189–205.

Morgan, W. J. (1971). Convection plumes in the lower mantle. *Nature* **230**, 42–43.

Morgan, W. J. (1972). Plate motions and deep mantle convection. In: Reginald, S., Hargraves, R. B., Morgan, W. J., Van Houten, F. B., Burk, C. A., Holland, H. D. & Hollister, L. C. (eds) *Studies in earth and space sciences: A memoir in honor of Harry Hammond Hess. Geological Society of America, Memoirs* **132**, 7–22.

Pik, R., Marty, B. & Hilton, D. R. (2006). How many mantle plumes in Africa? The geochemical point of view. *Chemical Geology* **226(3–4)**, 100–114.

Rehkämper, M. & Hofmann, A. W. (1997). Recycled ocean crust and sediment in Indian Ocean MORB. *Earth and Planetary Science Letters* **147**, 93–106.

Rogers, N., Macdonald, R., Fitton, J. G., George, R., Smith, M. & Barreiro, B. (2000). Two mantle plumes beneath the East African Rift system; Sr, Nd and Pb isotope evidence from Kenya Rift basalts. *Earth and Planetary Science Letters* **176(3–4)**, 387–400.

Rogers, N. W. (1993). The isotope and trace element geochemistry of basalts from the volcanic islands of the southern Red Sea. In: Prichard, H. M., Alabaster, T., Harris, N. B. W. & Neary, C. R. (eds) *Magmatic Processes and Plate Tectonics*. Geological Society, London: Special Publications **76**, 455–467.

Rooney, T., Furman, T., Yirgu, G. & Ayalew, D. (2005). Structure of the Ethiopian lithosphere: Xenolith evidence in the Main Ethiopian Rift. *Geochimica et Cosmochimica Acta* **69(15)**, 3889–3910.

Rooney, T., Furman, T., Bastow, I. D., Ayalew, D. & Gezahegn, Y. (2007). Lithospheric modification during crustal extension in the Main Ethiopian Rift. *Journal of Geophysical Research, B, Solid Earth and Planets* **112**, B10201, doi:10.1029/2006JB004916.

Rooney, T. O. (2010). Geochemical evidence of lithospheric thinning in the southern Main Ethiopian Rift. *Lithos* **117(1–4)**, 33–48.

Rooney, T. O., Bastow, I. D. & Keir, D. (2011). Insights into extensional processes during magma assisted rifting: evidence from aligned scoria cones and maars. *Journal of Volcanology and Geothermal Research* **201(1–4)**, 83–96.

Ryan, W. B. F., Carbotte, S. M., Coplan, J. O., O'Hara, S., Melkonian, A., Arko, R., Weissel, R. A., Ferrini, V., Goodwillie, A., Nitsche, F., Bonczkowski, J. & Zemsky, R. (2009). Global Multi-Resolution Topography synthesis. *Geochemistry, Geophysics, Geosystems* **10**, Q03014, doi:10.1029/2008gc002332.

Salters, V. J. M. & White, W. M. (1998). Hf isotope constraints on mantle evolution. *Chemical Geology* **145**, 447–460.

Saunders, A. D., Jones, S. M., Morgan, L. A., Pierce, K. L., Widdowson, M. & Xu, Y. G. (2007). Regional uplift associated with continental large igneous provinces: The roles of mantle plumes and the lithosphere. *Chemical Geology* **241**, 282–318.

Scarsi, P. & Craig, H. (1996). Helium isotope ratios in Ethiopian Rift basalts. *Earth and Planetary Science Letters* **144(3–4)**, 505–516.

Schilling, J.-G. (1973a). Iceland mantle plume: geochemical evidence along Reykjanes Ridge. *Nature* **242**, 565–571.

Schilling, J. G. (1973b). Afar Mantle Plume—rare-earth evidence. *Nature, Physical Science* **242(114)**, 2–5.

Schilling, J. G. (1985). Upper mantle heterogeneities and dynamics. *Nature* **314(6006)**, 62–67.

Schilling, J. G., Kingsley, R. H., Hanan, B. B. & Mccully, B. L. (1992). Nd–Sr–Pb isotopic variations along the Gulf of Aden—Evidence for Afar mantle plume continental lithosphere interaction. *Journal of Geophysical Research: Solid Earth* **97(B7)**, 10927–10966.

Shervais, J. W. & Hanan, B. B. (2008). Lithospheric topography, tilted plumes, and the track of the Snake River–Yellowstone hot spot. *Tectonics* **27(5)**, TC5004, doi:10.1029/2007TC002181.

Sleep, N. H. (2008). Channeling at the base of the lithosphere during the lateral flow of plume material beneath flow line hot spots. *Geochemistry, Geophysics, Geosystems* **9**, Q08005, doi:10.1029/2008GC002090.

Sleep, N. H., Ebinger, C. J. & Kendall, J.-M. (2002). Deflection of mantle plume material by cratonic keels. In: Fowler, C. M. R., Ebinger, C. J. & Hawkesworth, C. J. (eds) *The Early Earth: Physical, Chemical and Biological Development*. Geological Society, London: Special Publications **199**, 135–150.

Snedecor, G.W. & Cochran, W.G. (1989). *Statistical Methods*. Ames: Iowa State University Press, 503 p.

Storey, M., Saunders, A. D., Tarney, J., Gibson, I. L., Norry, M. J., Thirlwall, M. F., Leat, P., Thompson, R. N. & Menzies, M. A. (1989). Contamination of Indian Ocean asthenosphere by the Kerguelen–Heard mantle plume. *Nature* **338**, 574–576.

Stracke, A., Hofmann, A. W. & Hart, S. R. (2005). FOZO, HIMU, and the rest of the mantle zoo. *Geochemistry, Geophysics, Geosystems* **6**, Q05007, doi:10.1029/2004GC000824.

Thompson, R. N. & Gibson, S. A. (1991). Subcontinental mantle plumes, hotspots and pre-existing thinspots. *Journal of the Geological Society, London* **148**, 973–977.

Todt, R. A. (1996). Evaluation of a ^{202}Pb–^{205}Pb double spike for high-precision lead isotope analysis. In: Basu, A. & Hart, S. (eds) *Earth Processes: Reading The Isotopic Code: Geophysical Monograph*. Washington DC: American Geophysical Union, pp. 429–437.

Trua, T., Deniel, C. & Mazzuoli, R. (1999). Crustal control in the genesis of Plio-Quaternary bimodal magmatism of the Main Ethiopian Rift (MER); geochemical and isotopic (Sr, Nd, Pb) evidence. *Chemical Geology* **155(3–4)**, 201–231.

USGS (2004). *Shuttle Radar Topography Mission 1 arc second scene unfilled, unfinished 2.0*. College Park, MD: Global Land Cover Facility, University of Maryland.

Van Calsteren, P. W. C., Harris, N. B. W., Hawkesworth, C. J., Menzies, M. A. & Rogers, N. W. (1986). Xenoliths from southern Africa: A perspective on the lower crust. In: Carswell, D. A., Hall, J. & Wedepohl, K. H. (eds) *The Nature of the Lower Continental Crust*. Oxford: Blackwell Scientific, pp. 351–362.

Volker, F., McCulloch, M.T. & Altherr, R. (1993). Submarine basalts from the Red Sea—New Pb, Sr, and Nd isotopic data. *Geophysical Research Letters* **20(10)**, 927–930.

Volker, F., Altherr, R., Jochum, K.-P. & McCulloch, M. T. (1997). Quaternary volcanic activity of the southern Red Sea; new data and assessment of models on magma sources and Afar plume–lithosphere interaction. *Tectonophysics* **278(1–4)**, 15–29.

Watts, A. B. (1976). Gravity and bathymetry in the central Pacific Ocean. *Journal of Geophysical Research* **81**, 1533–1553.

Wendt, J. I., Regelous, M., Niu, Y. L., Hekinian, R. & Collerson, K. D. (1999). Geochemistry of lavas from the Garrett Transform Fault: insights into mantle heterogeneity beneath the eastern Pacific. *Earth and Planetary Science Letters* **173(3)**, 271–284.

White, W. M. & Hofmann, A.W. (1982). Sr and Nd isotope geochemistry of oceanic basalts and mantle evolution. *Nature* **296(5860)**, 821–825.

White, W. M., Albarède, F. & Télouk, P. (2000). High-precision analysis of Pb isotope ratios by multi-collector ICP-MS. *Chemical Geology* **167**, 257–270.

Willbold, M. & Stracke, A. (2010). Formation of enriched mantle components by recycling of upper and lower continental crust. *Chemical Geology* **276**, 188–197.

WoldeGabriel, G., Aronson, J. L. & Walter, R. C. (1990). Geology, geochronology, and rift basin development in the central sector of the Main Ethiopia Rift. *Geological Society of America Bulletin* **102(4)**, 439–458.

Wolfenden, E., Ebinger, C., Yirgu, G., Deino, A. & Ayalew, D. (2004). Evolution of the northern Main Ethiopian rift: birth of a triple junction. *Earth and Planetary Science Letters* **224(1–2)**, 213–228.

Zindler, A. & Hart, S. (1986). Chemical geodynamics. *Annual Review of Earth and Planetary Sciences* **14**, 493–571.

APPENDIX

TERNARY MIXING MODEL

The isotope composition of a multi-component mixture is a weighted average of the components contributing to the mixture:

$$R_{\mathrm{m}} = \sum c_i w_i R_i / \sum c_i w_i \qquad (1)$$

where R is the isotope ratio (of Pb, Nd or Sr), subscript i refers to component a, b or c (here a indicates the Afar plume, b depleted mantle, c Pan-African lithosphere), m is the mixture (sample), c_i is the Pb, Nd, or Sr concentration in component i, and w_i is the mass fraction contributed by each component i to the mixture.

We also have the closure condition

$$\sum w_i = w_a + w_b + w_c = 1. \qquad (2)$$

Therefore, when all end-member R_i and c_i values are known, the measurement of two isotope ratios (such as $^{206}\mathrm{Pb}/^{204}\mathrm{Pb}$ and $^{143}\mathrm{Nd}/^{144}\mathrm{Nd}$) for any sample leads to three equations (one for each R_{m}, plus the closure equation) and three unknowns (w_i values), and the system is fully solvable.

The chosen elemental concentrations and isotopic end-members are identical to those of Schilling et al. (1992), except the plume component, which was given a value corresponding to the C mantle reservoir (Hanan & Graham, 1996). A rationale for the end-member isotopic compositions has been given in the text and by Schilling et al. (1992). The derivation of the mixing model, rationale, and method for determining the end-member concentrations have been given in detail by Schilling et al. (1992, appendix).

Table A1: Major and trace element data for samples from the Wonji Fault Belt following the methods outlined by Furman et al. *(2006)*

Location	Lat. (°N)	Long. (°E)	Distance* (km)	SiO$_2$	MgO	CaO	MnO	TiO$_2$	Fe$_2$O$_3$	Na$_2$O	Al$_2$O$_3$	K$_2$O	P$_2$O$_5$	Rb	Sr	Ba	Zr	Y
WFB-N-14	8·76	39·61	340	47·01	6·67	11·34	0·16	2·11	11·39	2·91	18·31	0·43	0·28	7·1	514	179	87	18·1
WFB-1026	9·48	40·20	238	47·16	5·42	9·70	0·23	3·14	14·28	3·44	15·07	0·65	0·63	14·1	395	246	159	31·3

	Cs	Hf	U	Th	Nb	Ta	Sc	Co	Ni	Cr	V	La	Ce	Pr	Nd	Sm	Eu	Gd	Tb	Dy	Ho	Er	Yb	Lu	Pb
WFB-N-14	0·05	2	0·26	0·97	15·5	0·94	28·9	46	64	90	306	11	25·2	3·5	15·3	3·59	1·42	4·01	0·66	3·32	0·62	1·69	1·42	0·21	1·1
WFB-1026	0·15	3·8	0·47	1·67	28·8	1·84	29·7	42	34	59	305	18·9	44·3	6·1	26·8	6·4	2·32	6·87	1·06	6·17	1·2	3·2	2·75	0·41	1·5

*Radial distance from Lake Abhe, Afar.

Table A2: Model mass proportions of the end-members for the Main Ethiopian Rift data from Table 1

Sample	% Afar plume using model:					% Depleted mantle using model:					% Pan-African lithosphere using model:				
	A	B	C	D	Av.	A	B	C	D	Av.	A	B	C	D	Av.
WFB-1023	33	31	31	37	33	57	61	61	49	57	10	8	8	14	10
WFB-1027	36	36	33	36	35	55	54	61	55	57	9	9	6	9	8
WFB-1026	41	39	37	41	40	52	54	57	51	54	8	7	5	8	7
WFB-E99-2	26	24	25	28	26	62	67	66	57	63	12	9	10	14	11
WFB-N-18	34	31	31	34	32	53	60	60	54	57	13	9	9	12	11
WFB-1037	24	22	24	27	24	63	70	65	56	64	12	8	11	16	12

(continued)

Table A2: Continued

Sample	% Afar plume using model:					% Depleted mantle using model:					% Pan-African lithosphere using model:				
	A	B	C	D	Av.	A	B	C	D	Av.	A	B	C	D	Av.
WFB-KO-12	30	28	29	34	30	57	61	60	50	57	13	11	11	17	13
WFB-KO-4B	38	35	34	39	36	51	56	57	49	53	12	9	9	13	11
WFB-N-20	37	35	n.a.	39	37	52	56	n.a.	49	52	11	9	n.a.	12	11
WFB-1035	27	26	27	31	28	61	65	62	54	61	12	9	11	15	12
WFB-N-22	46	41	41	44	43	44	52	53	47	49	10	7	6	9	8
WFB-N-15	30	30	28	34	31	58	59	63	51	58	12	11	9	15	12
WFB-1036	37	35	35	38	36	53	57	56	50	54	11	9	9	12	10
WFB-N-21	27	26	26	31	28	61	63	64	53	60	12	10	10	16	12
WFB-E99-20	31	29	n.a.	33	31	57	62	n.a.	52	57	12	9	n.a.	14	12
WFB-N-01	23	21	23	27	24	63	69	64	53	62	13	10	13	20	14
DZ-1003	11	10	12	12	11	71	81	68	67	72	18	9	20	21	17
DZ-1004	23	20	22	22	22	63	72	67	67	67	13	8	11	11	11
DZ-1005	15	14	15	15	15	71	77	71	72	73	13	9	13	13	12
DZ-1013	18	16	18	18	17	70	76	70	69	71	12	8	12	13	11
DZ-1014	24	22	23	25	24	66	71	68	64	67	10	7	9	11	9
DZ-1009	21	19	21	24	21	68	74	68	61	67	11	7	11	15	11
DZ-1007	18	16	18	18	18	70	75	70	69	71	12	8	12	12	11
DZ-1008	21	19	21	21	21	68	73	68	68	69	11	8	11	11	10
BJ-1044	20	19	21	21	20	71	76	69	70	72	8	5	9	9	8
BJ-1048	10	9	11	11	10	80	84	78	78	80	9	6	11	12	10
BJ-1049	13	11	14	13	13	78	83	74	78	78	9	5	12	9	9
BJ-1051	19	18	20	20	19	72	77	70	71	73	8	6	9	9	8
BJ-1045	21	19	22	21	21	70	75	68	70	71	9	6	10	9	9
BJ-1053	21	19	22	21	21	70	76	67	70	71	9	6	11	9	9
BJ-1043	17	16	19	18	18	74	78	70	71	73	9	6	11	10	9

n.a., no data exist for one or more of the isotopes necessary to complete this system. Av. is the average of the four models and is used to plot Fig. 7. Model $A = ^{207}Pb/^{204}Pb–^{206}Pb/^{204}Pb$, Model $B = ^{208}Pb/^{204}Pb–^{206}Pb/^{204}Pb$, Model $C = ^{143}Nd/^{144}Nd–^{206}Pb/^{204}Pb$, Model $D = ^{87}Sr/^{86}Sr–^{206}Pb/^{204}Pb$.